

A WIDE FIELD HUBBLE SPACE TELESCOPE STUDY OF THE CLUSTER CL0024+16 AT $Z = 0.4$. I: MORPHOLOGICAL DISTRIBUTIONS TO 5 MPC RADIUS

TOMMASO TREU¹, RICHARD S. ELLIS¹, JEAN-PAUL KNEIB^{1,2}, ALAN DRESSLER³, IAN SMAIL⁴,
OLIVER CZOSKE^{2,6}, AUGUSTUS OEMLER³, PRIYAMVADA NATARAJAN⁵

Draft version October 29, 2018

ABSTRACT

We describe a new wide field Hubble Space Telescope survey of the galaxy cluster CL0024+16 ($z \approx 0.4$) consisting of a sparse-sampled mosaic of 39 Wide Field and Planetary Camera 2 images which extends to a cluster radius of ~ 5 Mpc. Together with extensive ground-based spectroscopy taken from the literature, augmented with over a hundred newly-determined redshifts, this unique dataset enables us to examine environmental influences on the properties of cluster members from the inner core to well beyond the virial radius (~ 1.7 Mpc). We catalog photometric measures for 22,000 objects to $I \gtrsim 25$ and assign morphological types for 2181 to $I = 22.5$, of which 195 are spectroscopically-confirmed cluster members. We examine both the morphology-radius (T-R) and morphology-density (T- Σ) relations and demonstrate sensitivities adequate for measures from the core to a radius of ~ 5 Mpc, spanning over 3 decades in local projected density. The fraction of early-type galaxies declines steeply from the cluster center to 1 Mpc radius and more gradually thereafter, asymptoting towards the field value at the periphery. We discuss our results in the context of three distinct cluster zones, defined according to different physical processes that may be effective in transforming galaxy morphology in each. By treating infalling galaxies as isolated test particles, we deduce that the most likely processes responsible for the mild gradient in the morphological mix outside the virial radius are *harassment* and *starvation*. Although more data are needed to pin down the exact mechanisms, *starvation* seems more promising in that it would naturally explain the stellar and dynamical homogeneity of cluster E/S0s. However, we find significant scatter in the local density at any given radius outside ~ 0.5 Mpc, and that the same T- Σ relation holds in subregions of the cluster, independent of location. In this hitherto unprobed region, where the potential of the cluster is weak, galaxies apparently retain their identities as members of infalling sub-groups whose characteristic morphological properties remain intact. Only upon arrival in the central regions is the substructure erased, as indicated by the tight correlation between cluster radius and Σ .

Subject headings: galaxies: clusters: individual (CL0024+1654) — galaxies: evolution — galaxies: formation — galaxies: photometry — galaxies: fundamental parameters

1. INTRODUCTION

Rich clusters offer an unique laboratory for studying the effects of the local environment on their constituent galaxies. Evidence has accumulated in recent years that environmental processes affect both the star formation and morphological characteristics of galaxies, the endpoint being the present-day morphology-density relation (Dressler 1980).

However, the nature and timescale of the relevant evolutionary processes remains unclear. As clusters represent concentrations of both dark and baryonic matter, the physical interplay between the observed properties of a galaxy and the cluster potential is likely complex. An important advance was the recognition that the hot intercluster gas observed in X-rays may significantly affect the star formation rate of recently-arrived infalling galaxies (Gunn & Gott 1972), possibly triggering star formation by compressing their gas clouds or quenching star formation by stripping their gas reservoir (Dressler & Gunn 1983; Byrd & Valtonen 1990; Evrard 1991; Fujita 1998; Abadi et al.

1999)

Much progress has followed the connection of Hubble Space Telescope (HST) imaging of clusters with deep ground based spectroscopy. The former is essential in providing galaxy morphologies at epochs where environmental processes can be witnessed, while the latter is essential in providing diagnostic information on the timescales of star formation and its recent truncation. The combination has been most powerful in understanding the origin of the increase with redshift in the fraction of blue members seen in cluster cores between $z = 0$ and $z \sim 0.4$ (Butcher & Oemler 1978, 1984). Several HST-based studies have demonstrated that the blue galaxies seen at $z > 0.3$ are largely star-forming spirals which are noticeably absent in present-day clusters. It has been proposed these are recent arrivals in the cluster, perhaps observed immediately prior to a removal of their gas supply. Importantly, some red cluster galaxies in the same clusters show evidence of recently truncated star formation (Dressler et al. 1994; Couch et al. 1994; Stanford, Eisenhardt & Dickinson

¹ California Institute of Technology, Astronomy, 105-25, Pasadena, CA 91125. tt@astro.caltech.edu; rse@astro.caltech.edu

² Observatoire Midi-Pyrénées, UMR5572, 14 Av. Édouard Belin, 31400 Toulouse, France

³ Carnegie Observatories, 813 Santa Barbara Street, Pasadena, CA 91101

⁴ Department of Physics, University of Durham, South Road, Durham DH1 3LE, UK

⁵ Department of Astronomy, Yale University, P.O. Box 208101, New Haven, CT 06250

⁶ Current address: Institut für Astrophysik und Extraterrestrische Forschung Auf dem Hügel 71, 53121 Bonn, Germany

1995).

The above cluster studies have been undertaken alongside similar HST-based campaigns devoted to the study of the *field galaxy population* (Glazebrook et al. 1995; Brinchmann et al. 1998; Cohen et al. 2000). Broadly speaking, these studies have likewise demonstrated an increase in gas content and star formation rate with redshift although mostly in lower mass systems than those discussed in the cluster studies. The extent to which the evolutionary trend seen in the field drives that observed in clusters is thus an interesting and relevant question.

Much of what has been learned thus far concerning the evolution of galaxies in clusters has been derived from detailed studies in the inner ~ 0.5 Mpc of several clusters, typically spanning a range in redshift (Smail et al. 1997; van Dokkum et al. 1998a; Oke, Postman & Lubin 1998). Only Couch et al. (1998) and van Dokkum et al. (1998b) secured morphological data beyond a radius of 1 Mpc via a WFPC2 mosaic. Although an efficient strategy in generating a large sample of spectroscopic members, information is only provided on the later states of the environmental processes. Important results have emerged including the relative abundances of elliptical and lenticular (S0) galaxies as a function of redshift (Dressler et al. 1997; Andreon et al. 1998; Fabricant et al. 2000) and the homogeneity in the colors of the E/S0 population (Ellis et al. 1997; Stanford, Eisenhardt & Dickinson 1998; van Dokkum et al. 2000).

A major problem that arises in developing a self-consistent evolutionary picture from observations made with a variety of clusters is the difficulty of assigning timescales to the phenomena observed, and connecting clusters at different redshifts into a temporal sequence. In fact, we have evidence that clusters evolve continuously by merging and accreting structures from the surrounding field (e. g. Zabludoff & Franx 1993; Abraham et al. 1996a; Balogh et al. 2000) as described in popular theories of structure formation (e. g. Kauffmann 1995a,b; Diaferio et al. 2001). Therefore, we cannot simply assume that a cluster observed for example at $z \simeq 0.6$ evolves “passively” to one observed at $z \simeq 0.4$.

Our approach in this series will be to secure high quality data for a single well-studied system over a large range in environmental density. A more secure connection with the evolution observed in field samples may thus be assured and, as we will demonstrate, the timescale of the star formation activities can be more readily determined, e. g. by estimating the likely dynamical trajectories of infalling galaxies. An important region which motivated the current study is that where infalling field galaxies first encounter the cluster potential and the intercluster gas. Few studies have been devoted to the investigation of this region either in a statistical sense for an ensemble of clusters (e.g. Balogh et al. 1999; Pimblet et al. 2002) or for individual clusters (Abraham et al. 1996a; Kodama et al. 2001).

In a seminal article, Abraham et al. (1996b) examined this region via moderate signal-to-noise ratio spectroscopy to ~ 5 Mpc in Abell 2390. An extensive wide-field redshift survey separating field and cluster members to large radius was central to progress in this respect enabling the

first measures of the radial gradients of diagnostic spectral features. Unfortunately, the spectroscopic data was marginal in terms of that required for studies of individual galaxies, and no HST data was available so a connection with morphology was not possible. Our series is concerned with developing and extending the analysis of Abraham et al. (1996b) for a single cluster, CL0024+16 ($z=0.4$), for which an extensive HST mosaic has been obtained. The present paper is primarily concerned with introducing and interpreting the morphological data enabled by our HST WFPC2 observations in the context of available spectroscopic data.

A plan of the paper follows: in §2 we summarize the scientific goals which motivate the series and, in turn, define the necessary observational data. We then introduce the observational data. In §3 we describe the strategy for the adopted HST observations, the data reduction techniques and the production of a catalog that will serve the entire survey. We define the basis of our morphological classifications performed to a limiting magnitude⁷ of $I = 22.5$ and discuss issues of completeness and bias. This catalog is merged with the available and new spectroscopic data in §4.

In preparation for the subsequent analysis of the data, in §5 we review the various physical mechanisms proposed to explain the relation between morphology and environment. An important output of this discussion which guides the later analysis are physical length scales and timescales associated with the various mechanisms which define how we will analyze and interpret the data in CL0024+16, both as a function of cluster radius and environmental density. In §6 we analyze the properties of the cluster galaxy population, both as a function of cluster centric radius and with local projected density, i.e. the T-R and T- Σ relations. Contrasting the trends seen in these two relations allows us to interpret the changes in morphology in the context of specific processes introduced in §5. Section 7 summarizes the results and our main conclusions.

Throughout the series, we assume the Hubble constant, the matter density, and the cosmological constant are $H_0 = 65 \text{ km s}^{-1} \text{ Mpc}^{-1}$, $\Omega_m = 0.3$, and $\Omega_\Lambda = 0.7$, respectively. Hence, at the distance of CL0024+16 ($z = 0.395$), $1''$ corresponds to 5.74 kpc, the bolometric distance modulus is $DM = 41.81$, and the look-back time is 4.6 Gyrs. Finally, r is the radial coordinate in 3-D space, while R is the radial coordinate in 2-D projected space.

2. A WIDE FIELD HST SURVEY OF CL0024+16

We are undertaking a wide-field HST survey, coupled with suitable ground-based spectroscopy, for a single cluster at intermediate redshift. The unique feature is adequate morphological and spectroscopic data from the core to the turnaround radius where field galaxies begin their infall. The key scientific goals are: to determine the mix of galaxy morphologies as function of cluster radius and local density; to measure the total cluster mass radial profile beyond the virial radius using weak lensing signals derived from background galaxies; to determine the star formation properties of cluster members via diagnostic spectroscopy; to connect these to their morphological and kinematic properties, and to interactions with the intercluster

⁷ All magnitudes are given in the standard Vega system.

medium (ICM); consolidate the above results via a unified picture for the transformation of the physical properties and morphologies of galaxies.

Whether such an ambitious list of goals can be uniquely realized via the detailed study of only a single cluster is of course unclear. Of necessity, given the challenge of obtaining such a wide body of HST and ground-based data, it is the logical place to start. Experience has shown that most astronomical objects/ systems when studied in considerable detail exhibit unforeseen peculiarities. For example, the progressive increase in dynamical data for local cluster galaxies has usually revealed that systems previously considered to be dynamically relaxed exhibit perceptible substructure (Dressler & Shectman 1988). Studies based on the statistical properties of member galaxies as a function of cluster radius must be analyzed with caution in such circumstances. This would argue for studying several targets and adopting some form of scaling law for combining data from different systems (van der Marel et al. 2000). On the other hand, at large radii, it is conceivable that substructures are a dominant feature of infall patterns which need to be understood rather than averaged out.

Cl0024+16 has a number of features that make it optimal for this study (c.f. Table 1). There is a wealth of observational data, including the extensive spectroscopic survey of Czoske et al. (2001). The choice of an intermediate redshift ($z \approx 0.4$) has many advantages. It ensures the presence of gas rich field galaxies whose infall is thought to influence the evolution observed in cluster cores. A large physical area can be observed with a relatively small number of WFPC2 pointings. Morphologies and high quality spectra of representative L^* galaxies can be obtained in economic exposure times with HST and Keck respectively. The cluster is also optimally placed along the line of sight to typical faint ($I \simeq 25$) background galaxies for the measurement and interpretation of weak lensing signals induced by the cluster. The presence of a multiply-imaged strong lensing feature of known redshift at the cluster center (Broadhurst et al. 2000) provides an important absolute calibration of the mass model.

We secured a large wide-field mosaic of HST images for Cl0024+16 through a dedicated program (HST Program 8559: PI Ellis). HST images were collected from Fall 2000 to Fall 2001 and form the subject of the first papers of this series, which describe the measurement of the mass profile of the cluster using the WFPC2 and STIS images (Kneib et al. 2003, in preparation), and the measurement of the size of the halos of cluster galaxies using galaxy-galaxy lensing methods (Natarajan et al. 2003, in preparation). Later papers will describe the results of further Keck spectroscopy of selected members as a means of investigating the star formation characteristics as a function of cluster environment.

3. THE WFPC2 IMAGING DATA

We now introduce the wide field WFPC2 imaging dataset for Cl0024+16. After defining the strategy which motivated the HST observations (§ 3.1), we describe the data reduction procedures (§ 3.2) which lead to two key products: a photometric object catalog (§ 3.3) with morphological classification (§ 3.4), which we will refer to as the WFPC2 catalog.

3.1. Observing Strategy

In order to probe both the transition and peripheral regions of the cluster (see § 5.2), a sparse-sampled pattern of WFPC2 fields was necessary. We defined a circle of diameter $\sim 25'$ (~ 10 Mpc) and arranged 38 non-contiguous pointings which, together with earlier archival data, fully cover the center and sample the periphery at $\simeq 30\%$ area coverage. This strategy ensures we cover the required range of environments and cluster radius for the galaxy population studies. The arrangement was also chosen to permit azimuthal-averaging of fields for radial trends, e.g. for the weak shear profile (c.f. Kneib et al. 2003 for a discussion of the observational strategy as defined from the lensing goals).

A list of pointings, coordinates and orientations is given in Table C2 and the field distribution is portrayed in Fig. 1. In the original approved schedule, the WFPC2 field positions and orientations were carefully chosen to ensure some overlap of parallel STIS observations. The higher spatial resolution of STIS can be used to great advantage in calibrating the WFPC2 point spread function for weak lensing studies. Unfortunately, for scheduling reasons, this carefully constructed plan had to be abandoned, and, in order to safeguard completing the survey prior to the launch of ACS, we had to discard all orientation restrictions on the WFPC2 pointings soon after observations commenced.

All WFPC2 images were taken in the F814W filter providing photometry for cluster members which approximates the rest-frame V-band (hereafter, for simplicity, we will refer to F814W as I). The filter choice was motivated by the need for an adequately faint sample of background galaxies for the weak lensing analyses, while ensuring adequate comparisons with existing and ongoing studies of intermediate redshift galaxies (e.g. Dressler et al. 1997; Brinchmann et al. 1998). At each position, four equal exposures totaling two HST orbits (4000s-4400s, see Tab C2) were dithered with a 2×2 grid with half-integer offsets. For the central field (POS00), we utilized the image originally analyzed by Colley et al. (1996) referred to in the Morphs collaboration (Smail et al. 1997) (GO: 5453, PI: Turner) whose exposure time was 18,000s in F814W and 25,200s in F450W.

3.2. Data Reduction

We implemented a pipeline based on the IRAF package DITHER (Fruchter & Hook 2002) to reduce the WFPC2 data. The pipeline cleans and combines the images, by iteratively refining the measurement of relative offsets and the cosmic rays/defect identification (the algorithm is similar to the one described by Fruchter & Mutchler 1998). The output of the pipeline consists of two sets of images, one with a pixel size equal to the original pixels size ($0''.1$ for the WF chips), and one with pixel size half the original ($0''.05$ for PC chips). An exposure time map is produced for each chip.

The quality of the combined images was carefully checked by visual inspection of all the intermediate steps of the pipeline and by a variety of quality checks including requirements on the homogeneity of the exposure time maps to ensure homogeneous photometry, and on the sharpness of the point spread function (the Gaussian-FWHM of stars

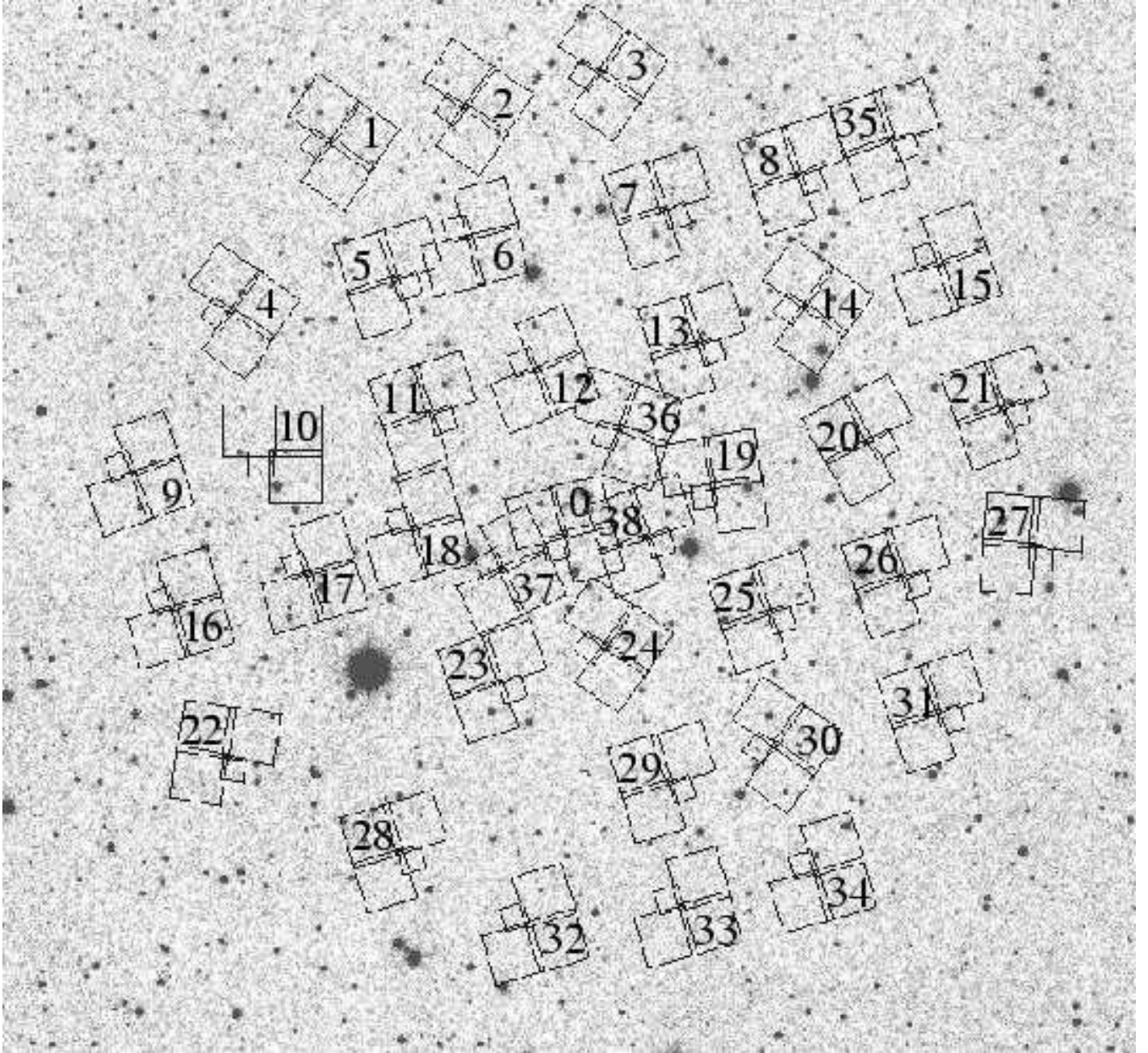


FIG. 1.— The arrangement of WFPC2 fields observed in Cl0024+16. The WFPC2 footprints are overlaid on a Digital Sky Survey image of the field (N is up, E is left). Each WFPC2 field is approximately $80''$ on a side. Details of each pointing are given in Table C2.

as measured with IMEXAM was generally slightly better in the combined images than in the original ones, due to better sampling).

3.3. The Photometric Catalog

The photometric catalog derived from the WFPC2 images will be used for most subsequent applications in the series of papers, from the morphological classification discussed later in this paper, to the identification of background samples for weak lensing studies (Kneib et al. 2003; Natarajan et al. 2003), and later for target selections for the spectroscopic campaigns. A reliable catalog with few spurious detections and well-understood completeness characteristics is essential. A high degree of completeness at the faintest limits ($I \gtrsim 25$) is less important than a well-understood completeness function because weak lensing signals depend on the angular size of a faint galaxy and cannot uniformly be detected in faint galaxies of a given apparent magnitude (e. g. Bacon, Refregier & Ellis 2000).

Faint object identifications were performed using the Source Extractor algorithm SExtractor (Bertin & Arnouts 1996), one of the standard packages for this purpose (e. g., Casertano et al. 2000). After some experimentation, it was decided to adopt detection criteria similar to those used by the Morphs collaboration⁸. The deblending threshold and contrast parameters were set to 32 and 0.03 respectively, ensuring nearby sources are separated while fainter objects that appear part of the same system (e. g., bright knots on spiral arms) are preserved as a single entity. These choices affect completeness somewhat at the faintest magnitudes – $I \gtrsim 25$ in our case – (c.f. discussion in Casertano et al. 2000), but will not affect the results discussed in this paper, which are mostly concerned with the brighter galaxies. The catalog does not include the area of reduced sensitivity covered by the PC which represents only a modest fraction of the total area.

A basic measure of catalog completeness can be determined from the I-band galaxy number counts after excluding duplications from overlapping fields (Fig. 2). Although obviously a clustered field, excluding the data from the central POS00, the CL0024+16 counts are only modestly above those of genuine field samples, mostly at $I \sim 20-22$; this gives a measure of the challenge of locating cluster members at large radii. The turnover fainter than $I \sim 25$ serves as an indicator of the limiting depth of our catalog. As expected, the central POS00 field (red stars) shows a more significant excess at magnitudes fainter than the brightest cluster galaxy (BCG; $I \sim 18$; see also Smail et al. 1997). The faster turnover of the central POS00 field at $I \gtrsim 25$ is the result of crowding, magnification bias (Fort et al. 1997; Dye et al. 2002), and possibly cosmic variance (see, e.g., Casertano et al. 2000).

As some fields overlap (see Fig. 1), we have an opportunity to verify photometric consistency. No systematic differences were found and the scatter is less than 0.05 mags rms at $I < 22.5$ increasing to $\sim 0.3 - 0.4$ mags at $I \sim 25$ rms. As expected, this rms scatter is slightly larger than the random error (0.2-0.3 mags) due to the additional systematic components in the detection algorithm and in the

computation of the total magnitude (mag_auto, see Bertin & Arnouts 1996). A $\sim 3\sigma$ detection at $I \sim 25$ is consistent with the observed turnover in the number counts. All HST images were registered to the astrometry of Czoske et al. 2001 (hereafter the CFHT astrometry), which has been determined to be accurate to $\lesssim 0''.2$ from comparisons with the USNO-A2.0 catalog. Offsets between the original WFPC2 astrometry and the CFHT astrometry are typically $\simeq 0''.5$, and in the overlap regions we find an rms scatter of $\sim 0''.3$, consistent with the estimated uncertainty in the CFHT astrometry.

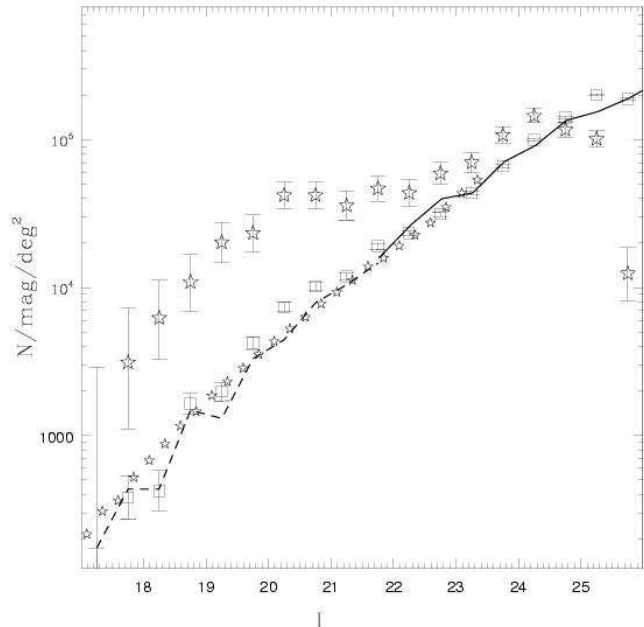


FIG. 2.— I-band number counts from the CL0024+16 photometric catalog (open red stars: central POS00 field; open black squares: remaining area) compared with data from the Hubble Deep Fields (solid line, Williams et al. 1996, Casertano et al. 2000) catalog, Postman et al. (1998; open stars) and the HST-Medium Deep Survey catalog by Abraham et al. (1996; dashed line). The turnover at $I \simeq 25.5$ indicates where the catalog becomes significantly incomplete.

The photometric catalog comprises 22,000 objects to $I \simeq 25$ ⁹. Entries are described in Tab C3 and the head of the catalog is given in Tab C4. In the central region, independent pointings partially overlap, and duplications have not been removed. All magnitudes are in the Vega system and corrected for galactic extinction, adopting $E(B-V)=0.057$ (Schlegel et al. 1998).

3.4. Morphological classification

We now discuss the morphological classification of the objects in the catalog. Broadly, the procedure followed that adopted for the HST *Medium Deep Survey* (Abraham et al. 1996a) for which the minimum typical exposure time (4000s) was similar and a limiting magnitude of $I=22.0$ was adopted. After some experimenting by one of the classifiers (RSE) in that study, it was determined that a similar degree of reliability would be achieved in the CL0024+16 fields to a fainter limit $I=22.5$. This value is

⁸ $0.12''$ above 24.6 mag arcsec⁻² for the WF chips, $0.09''$ above 23.6 mag arcsec⁻² for the PC. Photometric zero points were taken from the HST Data Handbook.

⁹ The catalog is available electronically at <http://www.astro.caltech.edu/tt/0024>

intermediate with the fainter limit ($I=23$) adopted in the 6300-16,800 sec Morphs study (Smail et al. 1997).

As noticed in previous studies, the uncertainty in the classification is a strong function of signal-to-noise ratio close to the limit and some distinctions are more critical than others, e. g. distinguishing amongst regular galaxies is more reliable than disentangling late types from merger and irregulars. Thus, after describing our classification procedure, we discuss in detail the uncertainty (§ 3.4.1). A summary is given in § 3.4.2.

Morphological classification of all objects with magnitude (mag_{auto}) brighter than $I = 22.5$ was performed by one of us (RSE) using an IRAF task which displayed, for each entry, a square region $12'' \times 8''$ on a side, on a logarithmic intensity scale to simulate appearance on a photographic plate. Each object was simultaneously displayed at four stretch levels to ensure an adequate dynamic range. Morphologies (hereafter T) were assigned according to the MDS scheme introduced by Abraham et al. (1996a): -2=star, -1=compact, 0=E, 1=E/S0, 2=S0, 3=Sa+b, 4=S, 5=Sc+d, 6=Irr, 7=Unclass, 8=Merger, 9=Fault. Examples for classes -2 to 8 are shown in Figures 3, and 4. It is important to clarify that the nomenclatures Sa+b and Sc+d represent the union of subclasses, not intermediate spiral types. As in the MDS, the system is hierarchical: classes such as E/S0 or S are used when the classifier recognizes the galaxy as an early or late type, but no further subclassification can be determined. The Unclass (7) category comprises objects that are only partially imaged, e.g. they fall on the edge of a chip. Finally, T=8 (Merger) is used when the isophotes of two objects of comparable brightness merge (c.f. examples in Fig 4). This could, of course, in some cases be due to projected alignments.

The classifier’s comments were also recorded together with the morphological type. A total of 2181 objects were processed in this way, including the ones in the central field classified by the Morphs collaboration. The distribution of morphological types as a function of magnitude (without regard to cluster membership) is shown in Figure 5.

3.4.1. *Uncertainties in the Morphological Classifications*

Internal consistency in our classifications can be obtained by examining the overlapping fields, given our IRAF task ensures a blind treatment of each image. At $I < 21$: 48 % of the galaxies have identical morphological type, 89 % differ by at most $\Delta T = 1$. At fainter magnitudes ($21 < I < 22.5$) 56 % of the galaxies have identical T, while 74 % differ by at most $\Delta T = 1$. No clear magnitude dependence is seen. If we consider only “broad classes”, defined as stars (T=-2), compacts (-1), early-types (E+S0, 0 to 2), spirals (3 to 5), and Irr/Unclass/Merger (6 to 8) galaxies, the consistency improves significantly. 75-80 % of galaxies have the same broad class and *all* lie within ± 1 broad class. The agreement is consistent with earlier similar studies (e. g. Smail et al. 1997; Fabricant et al. 2000).

A further step was undertaken to ensure internal consistency. Postage stamps $12'' \times 8''$ on a side were sorted by morphological type and magnitude and carefully examined by two of us (RSE and TT). By comparing images of comparable signal-to-noise, the consistency and repeatability of the classification was re-examined. Types were only

changed in $< 10\%$ of the galaxies, mostly within broad classes (e.g. Sa+b to S).

Two of the well-known critical points in the morphological classification, are E+S0 vs spiral separation, and star galaxy separation (see e. g. Smail et al. 1997; Fabricant et al. 2000). The difficulty of separating E+S0 and spirals has been discussed widely in the literature. Unfortunately – as opposed to the star galaxy separation where spectroscopic information provides an unambiguous verification – using external information to verify E+S0 vs spirals morphologies is much more difficult. Although certain properties, such as spectral features and colors, are known to correlate with morphology there is significant scatter, and, as we are interested in the stellar population properties of galaxies, their use could lead to significant biases when applied to evolutionary studies.

Distinguishing features (spiral arms, bright young stars and star forming regions) may be lost at intermediate redshift because of surface brightness dimming ($\propto (1+z)^{-4}$) and resolution and/or sampling effects. Figures 3 and 4 show that bright E+S0 and Sa+b galaxies can be separated brighter than $I \lesssim 20$. Our classifications are internally consistent to $I \sim 21$ but suffer some ambiguity at $I = 21 - 22.5$. As an external check, the study by Fabricant et al. (2000) of Cl1358+62 is particularly relevant since the HST observational setup (instrument, filter, and exposure time) and cluster redshift are closely similar to those for Cl0024+16. Fabricant et al. found that human classifiers consistently distinguish early-types and spirals to $I \sim 21$, with increasing uncertainty beyond this limit. Finer classification was found to be much more uncertain. For example the two classifier groups in Fabricant et al. (2000) yielded discrepant values of the ratio of S0 and E galaxies already at $I < 21$. We conclude that early-type and spiral galaxies can be consistently distinguished with our instrumental setup down to at least $I \sim 21$.

Two further effects should be considered. Firstly, if the distribution of morphological types is not uniform, any scatter might smear the distribution by transferring objects from the most populated class to adjacent classes (see e.g. discussion in the Appendix of Fabricant et al. 2000). The second is due to the specific effects of distance, i.e. loss of resolution and surface brightness dimming. Qualitatively, these effects tend to suppress low surface brightness features (such as extended envelopes around S0 galaxies) and smear out small-scale features (such as compact star forming regions, or spiral arms). Thus, the net qualitative effect is to transfer S0 galaxies to the E class and Sa+b galaxies to the S0 or E class. Unfortunately, the magnitude of these biases depend strongly on the properties of the parent populations and therefore cannot be accurately corrected without additional assumptions. However, in our observing conditions, these effects are likely to be small especially at $I \lesssim 21$ (see, e.g., discussion in Glazebrook et al. 1995; Abraham et al. 1996a; Ellis et al. 1997).

Securing a reliable distinction between stars, compact galaxies, and faint ellipticals is also an important concern. At bright magnitudes ($I \lesssim 20$) distinguishing between these types is straightforward (Figure 3). Fainter than $I \sim 20$, diffraction spikes cannot be seen and peaked nuclear emission might be present in some galaxies. Classi-

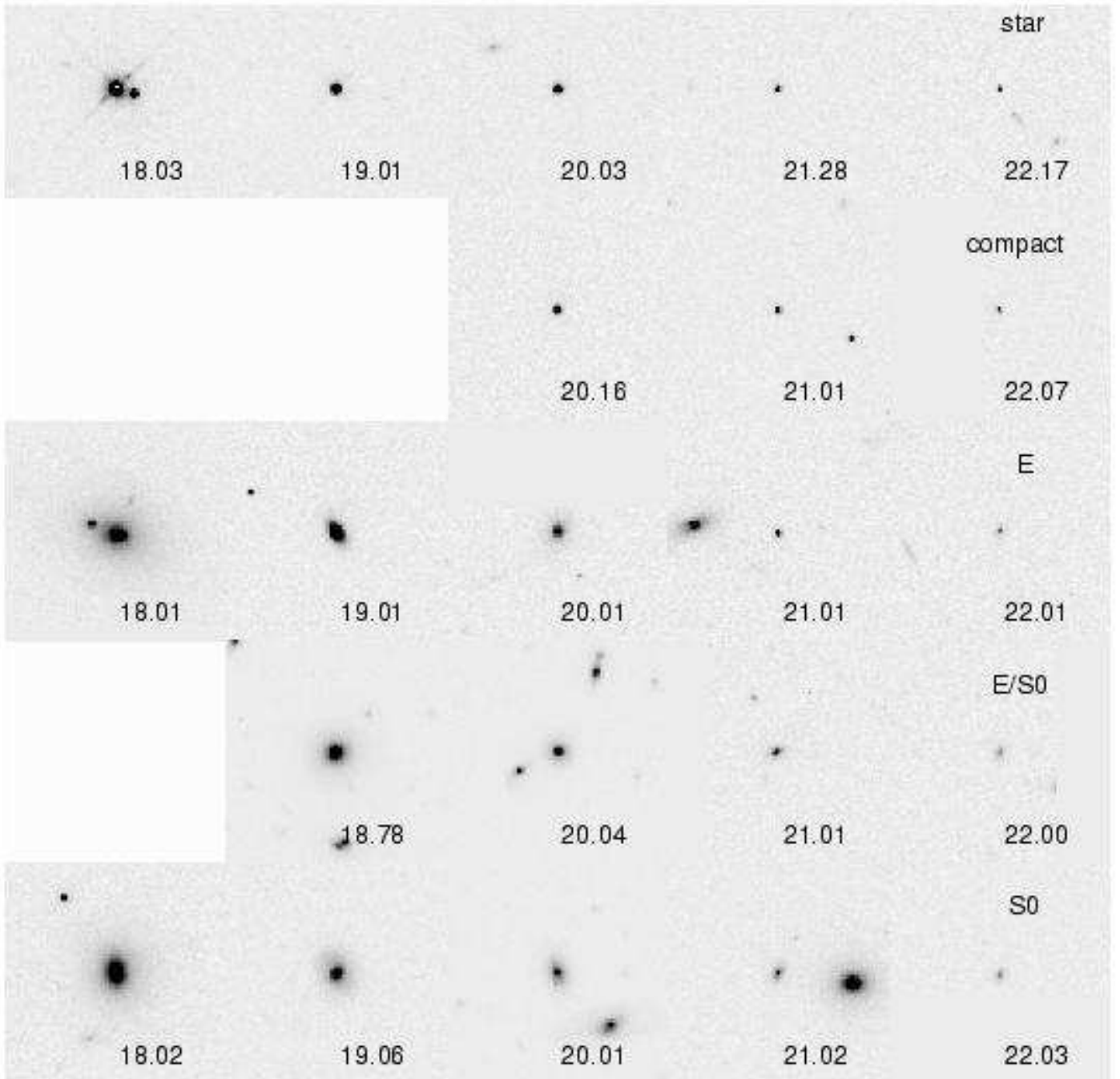


FIG. 3.— Montage of galaxies (each $12''/8$ on a side) in the CL0024+16 field sorted by type and magnitude. In each row we show typical galaxies for a given morphology, from $I \sim 18$ to $I \sim 22$ (left to right) in steps of ~ 1 magnitude. Empty spaces indicate no galaxy of that type is available in the respective magnitude bin. Magnitudes are indicated at the lower right corner of each image, morphological types at the top-right corner of each row. The display scale is linear, with uniform stretch levels.

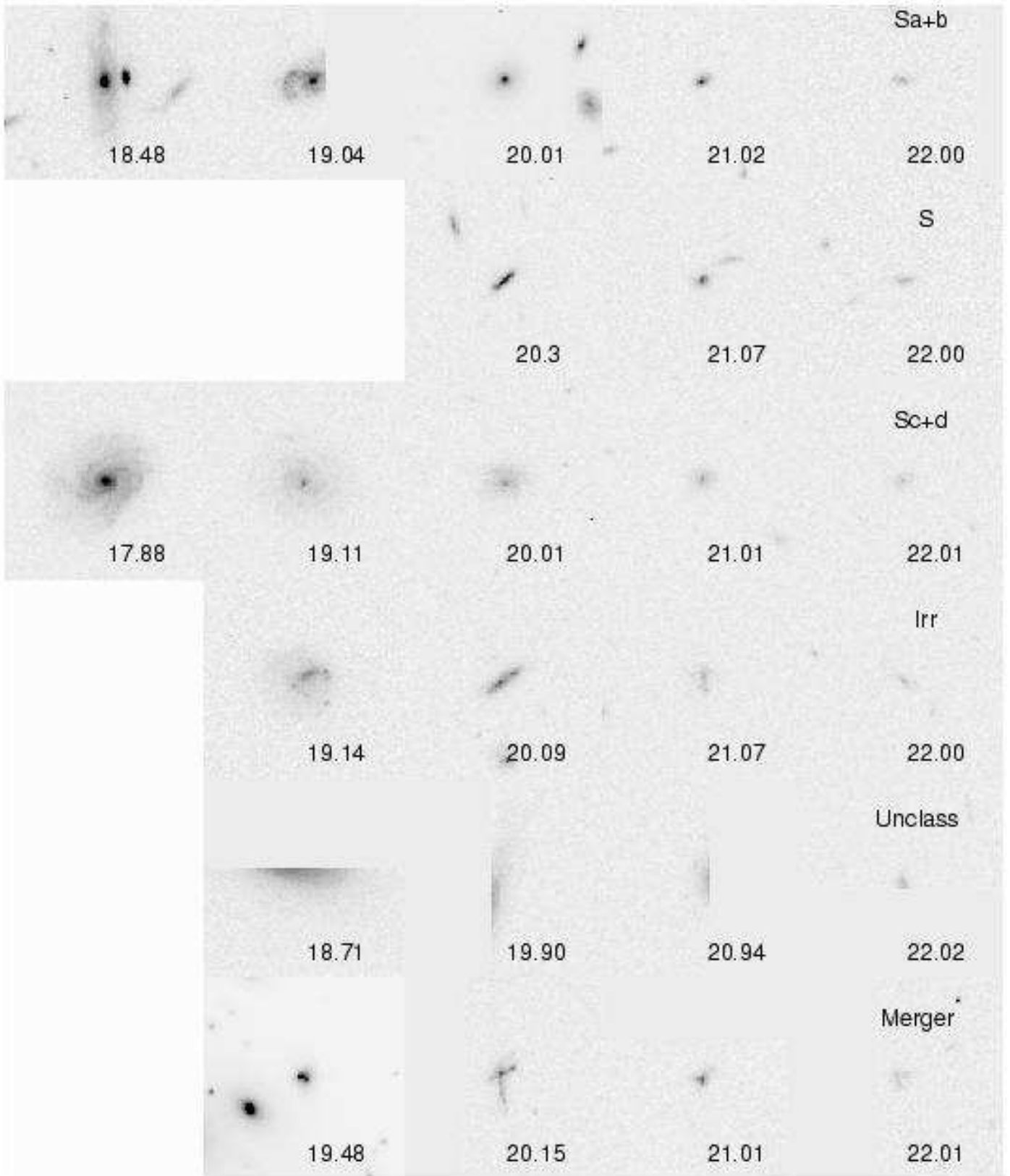


FIG. 4.— As Figure 3 for morphological types Sa+b (3) to Mergers (8).

fication becomes troublesome for objects smaller than the WFPC2 F814W PSF whose $\text{FWHM} \approx 0''.15$ (Casertano et al. 2000), corresponding to approximately 0.9 kpc at the cluster redshift. Fortunately, most normal elliptical members at $z \simeq 0.4$ within our magnitude limit should have effective radii significantly larger than 0.5 kpc (Ziegler et al. 1999 and references therein), and therefore should be clearly resolved.

Our spectroscopic catalog (see § 4) provides a valuable external check on the star compact elliptical boundary: out of 13 objects classified as stars with available spectroscopic data, 11 are confirmed and 2 have $z \sim 0.3$ flagged with “uncertain” quality. Out of 8 objects with spectra classified as compacts (i.e. deduced morphologically to be non-stellar), 5 are stars and 3 are galaxies with $z \approx 0.3 - 0.7$. Although the samples are small, the spectroscopic data suggests we have erred on the side of trying not to omit any extragalactic sources. This augurs well and suggests no ellipticals have been misclassified as stars. Indeed, all of the objects with zero spectroscopic redshift were independently morphologically classified as stars or compacts.

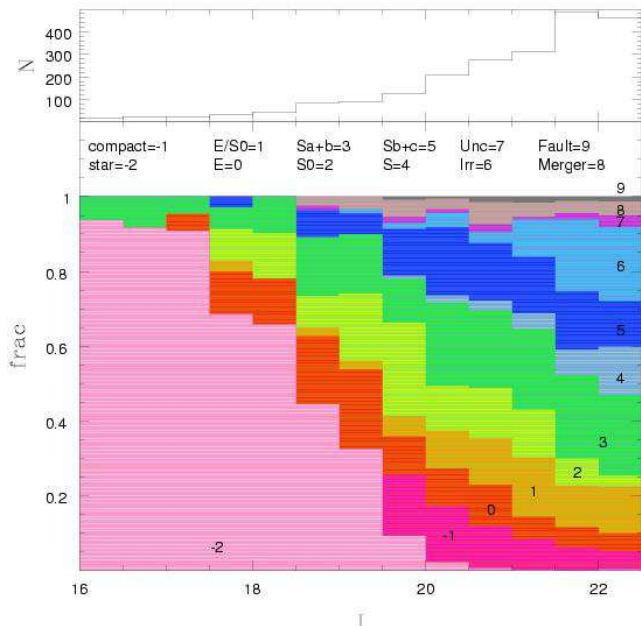


FIG. 5.— The distribution of morphological types as a function of I magnitude in the field of CL0024+16; no distinction is made between members and non-members.

A second external check is facilitated by considering the photometric distribution of objects in the color-magnitude diagram. For this purpose we augmented the HST photometry with wide field V and I band images obtained with Canada France Hawaii (CFHT) 12K camera. The E+S0 members define a tight color-magnitude sequence (see Natarajan et al. 2003). Stars span a wider range, generally bluer than the E+S0 red-sequence, and are found at significantly brighter magnitudes. Compacts are numerous only at $I \gtrsim 20$, and also span a wide range of colors although are generally redder than the E+S0 red sequence, indicating that some are likely to be background galaxies.

A final check is provided by the SExtractor param-

eter CLASS_STAR (see Bertin & Arnouts 1996 for details), which should be close to unity for genuine stellar objects and around 0 for extended objects. Confirming the results of our discussion, non-saturated stars have CLASS_STAR parameters greater than 0.9, while E galaxies have typically CLASS_STAR close to zero, except for a small fraction at magnitudes fainter than $I \sim 21$ that have CLASS_STAR larger than 0.8. Compacts have CLASS_STAR parameters between 0.8 and 1. In summary therefore, external diagnostic information based on spectroscopy and colors support the notion that there is little or no confusion so far as our morphological selection of cluster spheroidals, and virtually all of the compacts are either stars or distant background galaxies.

3.4.2. Summary of the morphological catalog

We have morphologically classified 2181 objects in the SExtractor catalog to a magnitude limit of $I < 22.5$, using the morphological classes illustrated in Figures 3 and 4. The resulting distribution of types as a function of magnitude is shown in Figure 5. The accuracy of the classification – measured in terms of repeatability – is found to be excellent down to $I \sim 21$, and still very good in broader classes (star; compact; E+S0; Sp; Irr/merger) to the limit $I = 22.5$, in agreement with the precision attained independently in similar datasets (Fabricant et al. 2000). Two critical points such as star/galaxy separation and S0 vs Sa separation are investigated with the aid of external information. We find that all of the spectroscopically confirmed stars are classified either as star or as compact, a class that is used mostly at magnitude fainter than $I \sim 20$, and is most likely a mix of stars, and high redshift compact objects. Similarly we conclude that the quality of the data is sufficient to separate reliably early-type and late-type galaxies down to at least $I \sim 21$. The subsequent analysis based on morphological types will note the distinction in quality beyond $I \sim 21$ and often be restricted to this limit where the classifications are particularly reliable.

4. THE SPECTROSCOPIC DATA

Following the comprehensive spectroscopic survey of Czoske et al (2001), a sufficiently large sample of spectroscopically confirmed members is already available to support the present investigation of the distribution of morphological types with radius and local density.

A spectroscopic survey of CL0024+16 is continuing at the 10m Keck telescopes with two goals: *i*) to obtain high-quality and where possible resolved 2-D spectra in order to explore dynamical and star formation characteristics for members of known morphology; *ii*) to extend the redshift survey beyond the limit of $I \sim 21$ of previous surveys (Dressler et al. 1999; Czoske et al. 2001) and gain a more complete sampling that is better matched to the dilute pattern of WFPC2 images. Although this survey will continue, we briefly present here the spectroscopic catalog incorporating all measures in the literature or made available to us, plus the initial results from our Keck campaign¹⁰.

The strategy, observations and analysis are discussed in Sec 4.1. The catalog is discussed in Sec 4.2. A separate discussion of the completeness of the catalog is given in Sec 4.3, bearing in mind the requirements for Section 6.

¹⁰ The complete redshift catalog will be released at the end of the campaign.

4.1. Keck Spectroscopy: strategy, observations & analyses

The new Keck spectra discussed here were obtained using the Low Resolution Imager Spectrograph (LRIS; Oke et al. 1995). In order to cover a suitable range of local density we decided to survey a strip oriented approximately North-South through the cluster center. The orientation was chosen to maximize overlap with WFPC2 fields with known cluster members.

Spectroscopic targets were selected from the CFHT I-band mosaic (Czoske et al. 2003, in preparation) according to the following priority: *i*) known members with HST morphology; *ii*) galaxies from the WFPC2 catalog without redshifts in the range $21 < I < 22.5$; *iii*) known members without WFPC2 imaging; *iv*) objects within $21 < I < 22.5$ without WFPC2 imaging. In the case of spectroscopically-confirmed members, where possible tilted slits were cut for those classified as edge-on spirals in order to offer the possibility of securing rotation curves from extended line emission. A detailed study of resolved spectroscopy will be deferred until a later paper, pending completion of the spectroscopic campaign. In this paper we use the newly determined redshifts to update the list of members.

Keck I LRIS observations were conducted on Oct 17-19 2001. For the red arm we mounted the 600/5000 grating providing wavelength coverage 5000 Å to 7500 Å with a pixel scale of approximately $1.25\text{Å} \times 0''.215$. The blue arm covered the region bluewards of 5100 Å with the 600/4000 grating and a pixel scale of approximately $1\text{Å} \times 0''.215$. Multi-object masks were milled with slitlets $1''$ wide providing spectral resolutions of $\sigma \sim 90 \text{ km s}^{-1}$ (red) and $\sigma \sim 130 \text{ km s}^{-1}$ (blue). Five masks were exposed yielding new data for 107 slitlets. The exposure time was $4 \times 1800\text{s}$ and the seeing was $0''.8 - 1''.2$ FWHM; conditions were generally non-photometric. After each set of four science exposures, internal flat field and Hg-Kr-Ne-Ar lamps were obtained without moving the telescope to obtain accurate fringing removal and wavelength calibration.

After bias removal the individual slitlets were separated and reduced in a standard manner (see e.g. Treu et al. 1999, 2001a). Extracted spectra were inspected by two of us (TT and RSE) and 92 redshifts measured by identifying absorption and emission lines (when present). A quality flag – in a scheme similar to that of Czoske et al. (2001) – was assigned to each spectrum: 1=secure (63 objects), 2=probable (12), 3=possible/uncertain (17). The latter category mostly includes spectra where only a single feature can be detected.

4.2. The Redshift Catalog

The Cl0024+16 redshift catalog is based on the new Keck data, the compilation from Czoske et al. 2001 (which includes Dressler et al. 1999 observations) and unpublished redshifts kindly provided by F. Owen (2001, private communication) and A. Metevier & D. Koo (2001, private communication). In total 1018 redshifts, including duplicates, are available, independently of the WFPC2 data. Duplications arise in several ways. For some galaxies, redshifts are available from more than one source. The typically agree to within 0.001; we adopt the average and the rms scatter as the uncertainty. Discrepant redshifts were found for only two galaxies which were removed from the combined catalog.

The final catalog comprises redshifts for 787 objects. As noted by Czoske et al. (2002), the distribution around $z \sim 0.4$ is characterized by a main peak (A in Fig. 6), a secondary peak at lower redshifts (B), interpreted by Czoske et al. (2002) as a foreground system, and a third sparser peak of galaxies at higher redshift. For a thorough discussion of this complex redshift distribution and possible interpretations see Czoske et al. (2002). Here we only remind that the relative velocity between the two peaks is $\sim 3000 \text{ km s}^{-1}$ in the rest frame of the cluster, and that the formal velocity dispersions of the two peaks are approximately 600 km s^{-1} . Adopting the velocity limits for the peaks as defined by Czoske et al. (2002), there are 304 galaxies in peak A ($0.387 < z \leq 0.402$) and 54 in peak B ($0.374 < z \leq 0.387$). Matching the above catalog with the WFPC2 catalog yields what we will term the WFPC2- z catalog containing 362 objects, including 15 stars. Of the galaxies with WFPC2 morphologies, 179 have redshifts within peak A but only 16 lie within peak B (Fig. 6). In the following we will use the term cluster members to refer to galaxies in either one of the two peaks (the results are unchanged if only peak A is considered).

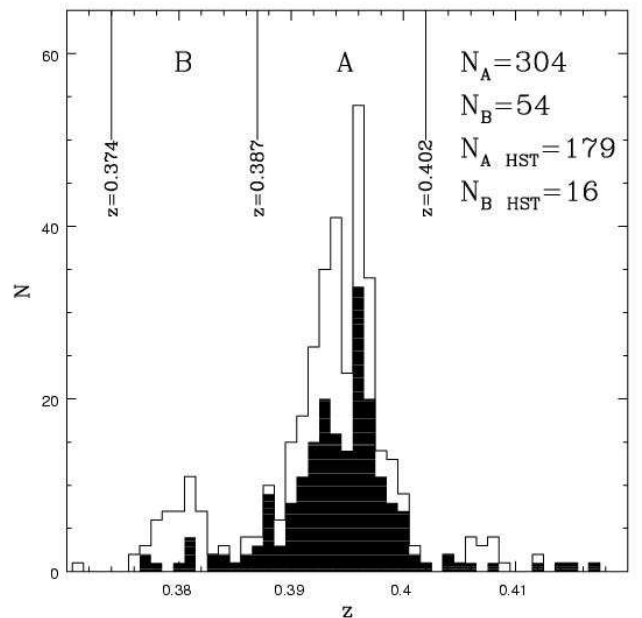


FIG. 6.— Redshift distribution of galaxies in the field of Cl0024+16 in the vicinity of $z \sim 0.4$. The distribution from the parent redshift catalog (Section 4.2) is shown as an empty histogram, while that from the WFPC2- z catalog is shown as a filled histogram. The double peak in the redshift distribution is discussed by Czoske et al. (2002).

Figure 7 shows the projected distribution of members in peaks A and B. As noticed by Czoske et al. (2002), those in peak B are fairly homogeneously distributed. By contrast, there is a marked clump of those in peak A to the NW of the cluster center. Because the fraction of area covered by our WFPC2 survey decreases with radius and the A peak is more concentrated than the B peak – the ratio of galaxies in peak B to galaxies in peak A is smaller in the WFPC2- z sample than in the full spectroscopic sample.

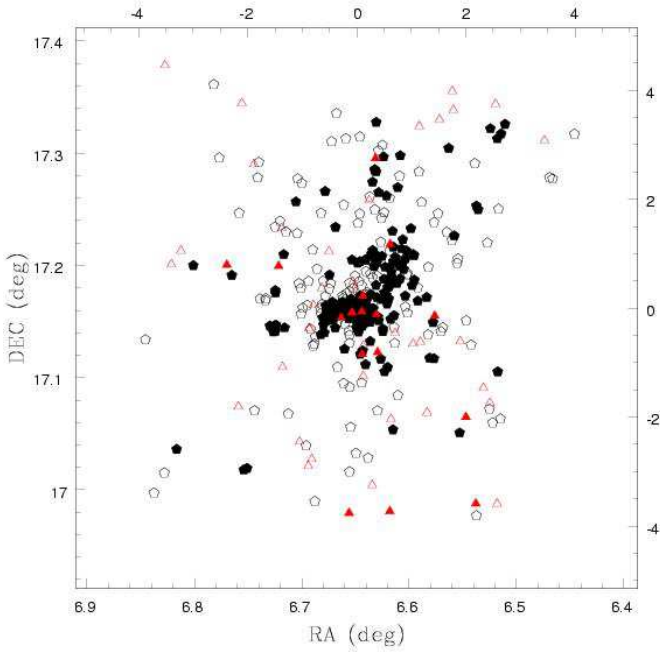


FIG. 7.— Projected distribution of CL0024+16 member galaxies (see text for details) in redshift peaks A (black pentagons) and B (red triangles). Solid symbols indicate objects with available HST-WFPC2 images. The top and right scale is in Mpc.

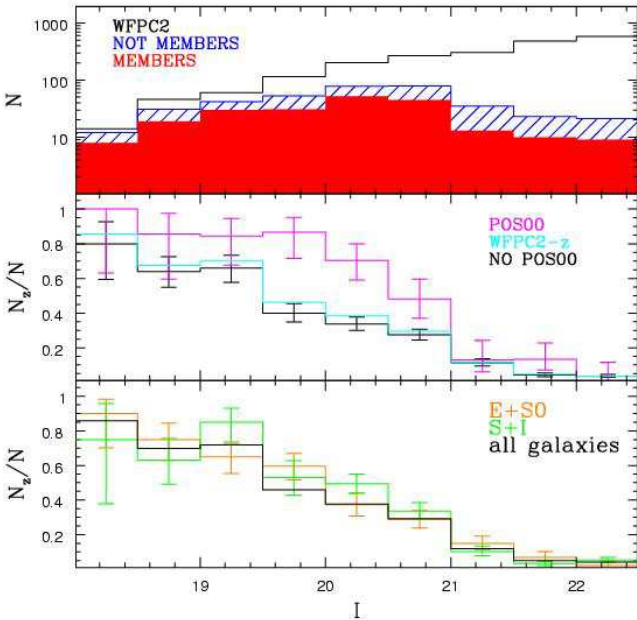


FIG. 8.— Completeness of the WFPC2-z catalog, as a function of I magnitude. Representative error bars are shown for reference. **Upper panel:** total number of galaxies, number of members ($0.374 < z \leq 0.402$), and number of non-members. **Middle panel:** redshift completeness, i.e. the fraction of galaxies with measured redshift, for the entire survey (WFPC2-z) and separately for the central POS00 field and the remainder of the survey (NO POS00). **Lower panel:** redshift completeness per broad morphological class.

4.3. Redshift Completeness

As the redshift catalog involves heterogeneous datasets, it is important to check redshift completeness in apparent magnitude, cluster radius and overall spatial extent.

First we examine completeness defined as the ratio of galaxies in the WFPC2-z catalog (N_z) to those in the $I < 22.5$ limited WFPC2 catalog, as a function of magnitude and cluster radius. The magnitude dependence is shown in the middle panel of Fig. 8. This is very high at bright magnitudes (especially for the central POS00 field), stays above 50 % until $I \sim 21$ and drops significantly beyond $I \sim 21$. The upper panel of the same figure shows the actual numbers per magnitude bin. Completeness does not depend significantly on the morphological type, as demonstrated in the lower panel of Fig.8. Accordingly, in the following analysis we assume that the WFPC2-z catalog is representative of the entire population without introducing significant bias in the mix of morphological types.

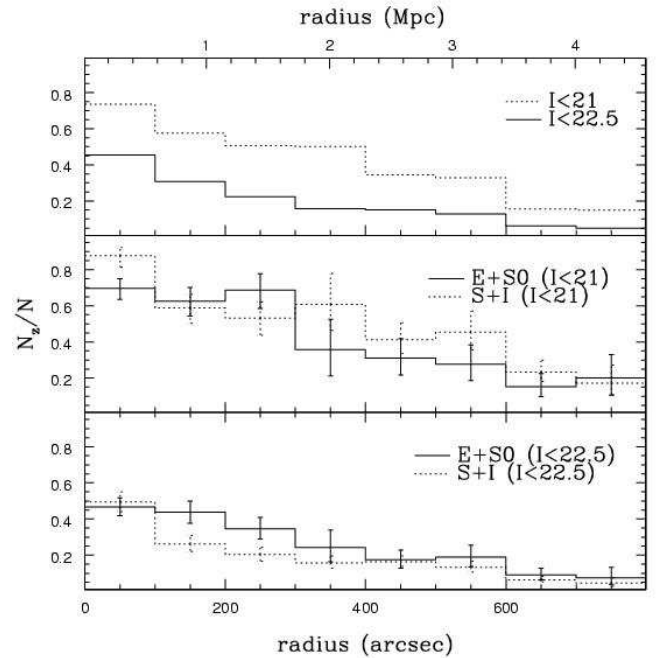


FIG. 9.— Redshift completeness of the WFPC2-z catalog as a function of cluster radius. On the top axis the scale in Mpc is shown for reference. Representative error bars are shown for reference. **Upper panel:** all morphological types. **Middle panel:** Per broad morphological type to $I < 21$. **Lower panel:** Per broad morphological type to $I < 22.5$.

Second, in Figure 9 we show the redshift completeness as function of cluster radius. At $I < 21$ the completeness drops sharply from almost 80 % at the center to below 20 % beyond $600''$ (~ 3 Mpc). At fainter magnitudes the completeness is significantly smaller, dropping below 20 % already at $300''$. Completeness as a function of radius segregated by broad morphological type is shown in the middle and lower panels of Figure 9. Importantly, no major difference is found at either faint or bright magnitude limits, confirming that the WFPC2-z catalog appears to be representative of the morphological mix at any given radius.

In summary, the WFPC2-z catalog is sufficiently complete at $I < 21$, particularly in the central Mpc where it is above 60%. It declines to 20 % at 5 Mpc. The completeness is much lower for galaxies fainter than $I = 21$; it is ~ 30 % for $I < 22.5$ in the central Mpc. Such incompleteness is inevitable even after considerable efforts. Fortunately, however, the catalog is not obviously biased in favor of any particular morphological type.

We will argue in the next sections that, by restricting the analyses to $I \sim 21$, uncertainties arising from both incompleteness and morphological typing (see § 3.4.1) are minimal. We will assume that the distribution of morphological types in the WFPC2-z sample is representative. It is recognized that at large radii (4-5 Mpc) – where spectroscopic information is most needed to establish membership – the WFPC2-z sample is only $\simeq 20\%$ of the parent sample, so significant extrapolation is necessary. Accordingly, results based on the WFPC2-z catalog in this region must be interpreted with greater caution.

5. THE PHYSICAL NATURE OF ENVIRONMENTAL EVOLUTION IN CLUSTER GALAXIES

Before interpreting the observations, it is convenient to build a physical framework for our study by defining the relevant time, velocity, and length scales associated with some of the various processes that have been proposed for the environmental evolution of cluster galaxies. We introduce these processes in Section 5.1. Since there exists a considerable literature on this subject with creative terminology often used with various meanings, we also use this opportunity to define our own terminology. Ideally we are interested in reconstructing the evolution of a single, hypothetical representative galaxy as it enters the cluster potential and interacts with the intercluster medium. To this aim, we present estimates of the sphere of influence of each relevant physical process affecting the infalling galaxy.

Using a simple cluster model and estimates of relevant length, time and velocity scales discussed in the Appendices, in Section 5.2 we discuss projection effects and use the various scales to define various observable regions of the cluster for each of the physical mechanisms listed in Section 5.1. The key output is a series of distinguishing zones which will form the basis of the later analysis.

5.1. Environmental Processes in Rich Clusters

For simplicity, we define the various processes under three broad headings: galaxy-ICM interactions (which refers to the interaction of a cluster galaxy with the gaseous component of the cluster), galaxy-cluster gravitational interaction (which includes tidal and related dynamical processes), and smaller-scale galaxy-galaxy interactions. Clearly the distinction is, in places, somewhat arbitrary.

1. Galaxy-ICM interactions. a) Ram pressure stripping, the removal of galactic gas by pressure exerted by the intercluster medium (Gunn & Gott 1972; Fujita 1998; Fujita & Nagashima 1999; Abadi et al. 1999; Toniazzo & Schindler 2001; Fujita 2001), serves to terminate star formation by removing the gas supply. b) Thermal evaporation of the galactic interstellar medium (ISM) by the hot ICM (Cowie & Songaila 1977). c) Turbulent and viscous stripping of the ISM (Nulsen 1982; Toniazzo & Schindler 2001). d) Pressure-triggered star formation in which galactic gas clouds are compressed by the ICM pressure thereby temporarily increasing the star formation rate (Dressler & Gunn 1983; Evrard 1991; Fujita 1998).

2. Galaxy-cluster gravitational interactions. a) Tidal compression of galactic gas (Byrd & Valtonen 1990; Henriksen & Byrd 1996; Fujita 1998) by interaction with the cluster potential can increase the star formation rate; b) Tidal truncation of the outer galactic regions (e.g. the dark matter halos) by the cluster potential (Merritt 1983, 1984; Ghigna et al. 1998; Natarajan et al. 1998). If tidal interactions remove the gas reservoir they can also lead to quenching of star formation but, more generally, such processes can be inferred via structural changes in the galactic mass profiles.
3. Galaxy-galaxy interactions. a) Mergers, i.e. low speed interactions between galaxies of similar mass (Icke 1985; Mihos 1995; Bekki 1998). b) Harassment, i.e. high speed interactions between galaxies in the potential of the cluster (Moore et al. 1996; Moore, Lake & Katz 1998; Moore et al. 1999).

Depending on the fraction of gas removed and its rate, ram-pressure stripping, thermal evaporation, turbulent and viscous stripping can lead either to a rapid quenching of star formation or a slow decrease in the star formation rate if only the loosely bound reservoir surrounding field galaxies is affected (Larson, Tinsley & Caldwell 1980, Balogh, Navarro & Morris 2000; Diaferio et al. 2001; Drake et al. 2000). Independent of the precise physical process, we will label this slow decrease in the star formation rate *starvation*.

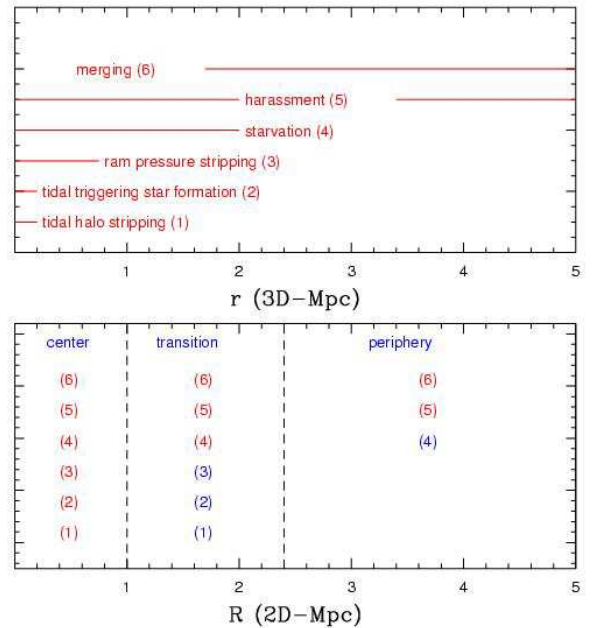


FIG. 10.— Summary of the regions where key physical mechanisms are likely to operate. Top panel: the horizontal lines indicate the radial region where the mechanisms are most effective (in 3-D space; note that harassment is effective in the entire range). Lower panel: for each projected annulus (as in Figure 12) we identify the mechanisms that can have affected the galaxy in the region (red). The blue numbers indicate processes that are marginally at work. For reference, the virial radius is $r_V \sim 1.7$ Mpc. See Section 6.2 for discussion.

The above mechanisms can affect the observed internal structure of cluster galaxies, including the mass distribu-

tion as probed by galaxy-galaxy lensing, internal kinematics as probed by resolved spectroscopy, and/or the star formation properties as probed with diagnostic spectroscopic and photometric features. Crucially, changes in internal structure and star formation properties can affect morphologies. In disentangling the various effects, we must attempt to rank – at least approximately – the importance of each mechanism for various physical regions of the cluster. The dominant physical mechanisms together with the estimate of their spheres of influence – as derived in Appendix B – are summarized in the upper panel of Figure 10.

5.2. Defining Diagnostic Cluster Regions

In order to explain the run of observables with radius in terms of the various physical mechanisms discussed, we use the spheres of influence shown in Figure 10 and the physical scales estimated in the Appendices, to determine how our instantaneous view of the observed position of the cluster galaxies may be linked to the physical and temporal scales of influence of each mechanism taking into account the effects of projection. Although galaxies can move significantly during transient phenomena of ~ 1 Gyr duration, the goal is to identify projected regions where we can *exclude* the possibility that certain mechanisms are at work. We define three annular projected regions: the cluster center, a transition region and the cluster periphery (shown in Figure 10, lower panel) within which we will search for correspondence in the observed properties of the galaxy population.

1. The central region comprises that within a ~ 1 Mpc radius. It is the region where the cluster potential is steepest and the ICM is detectable. Most of the mechanisms are effectively at work (see Figure 10, lower panel), speeds can be high (up to a few thousands of km s^{-1}), and projection effects can pollute this central region with galaxies that are at the periphery of the cluster. Hence unfortunately none of the mechanisms can be definitely excluded, although we can expect the mechanisms mostly related to the cluster potential (tidal stripping and tidal triggering) to be dominant. This is also the region mostly probed by previous HST surveys.
2. The transition region - an annulus between ~ 1 and 2.4 Mpc comprising the virial radius – is sufficiently far from the center that galaxies observed in this region cannot have experienced tidal effects more recently than 0.5-1 Gyr ago and cannot be experiencing ram-pressure stripping (although they can have in the recent past).
3. The periphery is the annulus between ~ 2.4 Mpc and the outermost radius probed (~ 5 Mpc). It is so far from the center (and speeds are lower than in the rest of the cluster) so that, given the discussion in Appendix C, we can safely assume that most of the galaxies at the periphery of the cluster *have never been through the cluster center* and therefore have never experienced the effects of tidal stripping, tidal triggering of star formation and ram-pressure stripping. Nevertheless, they may be experiencing

starvation and are able to undergo mergers or be harassed by massive nearby galaxies.

6. THE MORPHOLOGICAL DISTRIBUTION IN CL0024

We now combine the morphological and the redshift catalogs to study the distribution of morphological types in CL0024+16 both as a function of radius (hereafter the T-R relation; Section 6.2) and as a function of the local projected density (hereafter the T- Σ relation; Section 6.3)

In the local Universe, the T- Σ and T-R relations have been actively studied over the past three decades (Oemler 1974; Melnick & Sargent 1977; Dressler 1980; Postman & Geller 1984; Giovanelli et al. 1986; Whitmore & Gilmore 1991; Oemler 1992; Whitmore, Gilmore & Jones 1993), often in terms of the quest for the most fundamental relation. Indeed, there is a strong scientific motivation for determining and comparing these relations over a wide range of environmental density in order to determine which physical processes fundamentally governs the morphological evolution of galaxies. For example, the T-R relation should provide a tool to investigate the effects of those phenomena which are related to the cluster’s gravitational potential including interaction with the hot intercluster medium: such phenomena should run broadly as a function of azimuthally-smoothed radius. On the other hand, the effects of local overdensities and subclustering in the resident or newcomer population, will be erased in the T-R analysis. In this case, it is useful to examine the T- Σ relation.

Dressler (1980) introduced the T- Σ relation as a means to investigate the environmental effects on galaxy evolution in non symmetric (“non-relaxed”) clusters, where the definition of a cluster center was difficult and ambiguous. Remarkably, Dressler (1980) found that the T- Σ relation in the local Universe was identical for “relaxed” and “non-relaxed” clusters (see also Dressler et al. 1997), and used this result to argue against ram-pressure stripping as a dominant mechanism to transform spirals into E+S0. Whitmore & Gilmore (1991) and Whitmore et al. (1993) reanalyzed the data in the Dressler’s sample applying several corrections to the background estimate, magnitude limit, and center estimate. They claimed that morphology correlates better with radius than with local density and since a sharp decrease in the fraction of E+S0 with radius is seen only in the innermost regions (~ 0.5 Mpc) they argued that tidal disruption of spirals and S0 by the cluster potential is the dominant mechanism.

Further insight can be gained by studying the T-R and T- Σ relation at intermediate redshift $z \sim 0.5$, where the galaxy population is undergoing profound transformations. Dressler et al. (1997) studied the T- Σ and T-R relations in the core (typically within the inner 0.5 Mpc) of a sample of clusters at $z \sim 0.3 - 0.5$ including CL0024+16. For the high concentration clusters – such as CL0024+16 – they found the fraction of early-type galaxies was a steeply increasing (decreasing) function of local density (radius). By contrast, the low concentration clusters did not show any gradient in the fraction of early-type galaxies with respect to local density or radius. Consequently they inferred that low concentration clusters are less evolved than high concentration ones and segregation of morphological types has not happened yet. Unfortunately, their data did

not cover the periphery of clusters, which we argue (Section 5) is helpful in understanding the mechanisms driving the change of the morphological mix between $z \sim 0.5$ and today (Dressler et al. 1994; Couch et al. 1994; Dressler et al. 1997).

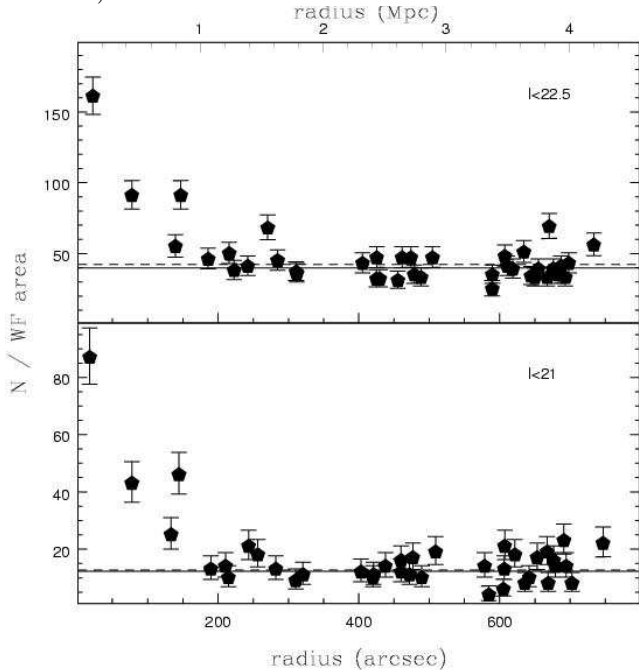


FIG. 11.— Average observed galaxy density per WFPC2 pointing in the Cl0024+16 field as a function of distance from the cluster center for two magnitude limits. The top axis shows the scale in Mpc. Error bars show the errors computed assuming Poisson noise. Solid and dashed lines indicate field number counts determined respectively by Abraham et al. (1996a) and Postman et al. (1998). Beyond ~ 1 Mpc the surface density approaches this value.

We wish to extend the T- Σ and T-R relations to larger radii (5 Mpc) and lower projected densities. As a laboratory for investigating this issue, Cl0024+16 is an interesting case because the two descriptions are not completely equivalent. Both the redshift distribution (Figure 6) and the projected distribution (Figure 7) indicate the cluster is not perfectly regular or relaxed (Czoske et al. 2002), notice in particular the overdensity NW of the center, with a somewhat poor correspondence between radius and projected density. These issues are shown quantitatively in Figure 11, where we plot the observed (not field-subtracted) average galaxy density per WFPC2 pointing as a function of cluster radius. Although an average trend is seen, there is considerable scatter (Section 6.3). Accordingly, contrasting galaxy properties in the context of both variables will be illuminating.

6.1. Measuring the T- Σ and T-R relations

In order to derive the T- Σ and T-R relations we must remove background/foreground contamination, compute the limiting magnitude and determine the cluster center. The ideal solution for resolving field contamination - the spectroscopic identification of all cluster members to our magnitude limit over the entire Cl0024+16 field - is beyond our current observational resources. Despite almost 800 redshifts, our WFPC2-z catalog is only 20 % complete at the periphery (Section 3). Achieving reasonable spectroscopic completeness over such a large area is certainly

a worthwhile goal within reach of the new generation of high-multiplexing spectrographs currently being commissioned on large telescopes (DEIMOS & IMACS on Keck and Magellan, for example). For now, we adopt a statistical approach based on the average field number counts. However, despite progress in measuring field counts (e.g. Postman et al. 1998; Casertano et al. 2000), the uncertainties are still significant for our purposes. In Figure 11 we plot both the I-band background surface density as measured by Abraham et al. (1996a) and Postman et al. (1998), to illustrate this uncertainty. The uncertainty is clearly relevant at large radii. Additionally, field galaxies are clustered on the angular scale of a WF chip (see also Valotto, Moore & Lambas 2001) thus field to field variation dominates the uncertainty in the background contamination.

To estimate the average background count per morphological type, we adopt the Postman et al. (1998) number counts, scaled by the fraction of morphological types found by Abraham et al. (1996a) at the corresponding limiting magnitude. For example the fraction of compact/E+S0/S (see below) are 5%:28%:49% at $I < 21$ and 10%:18%:43% at $I < 22.5$. This procedure combines the advantage of having the large area used by Postman et al. (1998) to determine the counts, with the background morphological distribution determined on the same scheme by the same classifier.

Another important issue is the computation of the limiting absolute magnitude. The catalog of local clusters used by Dressler et al. (1980) is limited to galaxies more luminous than $M_V = -20.4$ ($H_0 = 50 \text{ km s}^{-1} \text{ Mpc}^{-1}$; see also Dressler et al. 1997 and references therein). This limit can be converted into an I-band apparent magnitude using,

$$M_V = I - DM + \Delta m_{V8}, \quad (1)$$

where the k -color correction (Treu et al. 2001a) $\Delta m_{V8} = 0.85 \pm 0.03$ is computed using a broad range of synthetic spectra (Bruzual & Charlot 1993; GISEL96 version) and empirical templates (Kinney et al. 1996). The uncertainty in the transformation is very small because, at the redshift of Cl0024+16, the F814W filter closely matches rest frame V . From Eq. 1 the apparent magnitude limit of the local morphology-density analysis by Dressler et al. (1980) corresponds to $I=21.13$.

Since a galaxy with $M_V = -20.4$ at $z=0$ most likely did not have the same luminosity at $z \sim 0.4$, it is important to consider corrections for luminosity evolution. For the E+S0 population, Fundamental Plane (Djorgovski et al. 1987; Dressler et al. 1987) studies indicate rest-frame V band brightening of $\sim 0.4 - 0.6$ mags by $z=0.4$ (van Dokkum & Franx 1996, Treu et al. 1999, 2001b; van Dokkum et al. 2001; Bernardi et al. 2003). The expected evolution for spirals is less clear, with reported measurements ranging from none to up to ~ 1 magnitude of brightening to $z \sim 1$ in rest-frame B (Lilly et al. 1998; Simard et al. 1999). Metevier, Koo & Simard (2002) have constructed the Tully-Fisher relation for 7 galaxies in Cl0024+16 and find no evidence for a change in the slope or intercept with respect to local samples. Clearly if these indications are correct and we ignored any luminosity correction, we would overestimate the fraction of early-type galaxies. Given the uncertainties, as in previous studies

we prefer to present the observations, neglecting evolution. Fortunately, our results are not particularly sensitive to changes of ~ 0.5 mags in the applied limit (changes within the errors; see also Dressler et al. 1997; Kodama & Smail 2001). Furthermore, we are particularly interested in the trends within one system, which are not affected by differential luminosity evolution.

Although CL0024+16 is centrally concentrated and approximately rotationally symmetric to the extent that a T-R analysis is justified, some asymmetry is seen, e.g. the overdensity to the NW. For consistency with previous studies we adopt the X-ray center as cluster center. However, we have repeated the analysis in the following sections adopting alternative centers (Table 1) and the results are robust, changing less than the error bars.

Finally, we will restrict ourselves to the broad morphological classification scheme which is robust at $I < 21.1$ (Section 3.4). This provides good statistics at low densities/large radii and enables us to perform better field subtraction. For simplicity we will refer to the broad morphological classes as compacts (C; T=-1), early-types (E+S0; 0-2), spirals (S; 3-5), and “irregulars” (I; 6). Finer classification, including the separation of E and S0 galaxies (see, e.g., Dressler et al. 1997, Andreon et al. 1998; Fabricant et al. 2000) will be deferred until a later paper.

6.2. Radial trends

6.2.1. Observations

We now discuss the observed radial trends in morphological types. There are three key issues. How far out in radius can we trace the cluster in our dataset? What is the run with radius of the density of E+S0 and S+I galaxies? How does the cluster population of CL0024+16 compare to the surrounding field?

The lower panel of Figure 12 shows the fraction of spectroscopic members (defined as that fraction of all with redshifts lying within $0.374 < z < 0.402$) as a function of radius. Error bars were obtained assuming the binomial distribution (Gehrels 1986). Clearly, there is an excess of galaxies to the largest radius (≈ 5 Mpc). Using the Canada France Redshift Survey Spectroscopic catalog (Lilly et al. 1995) limited at $I < 21.1$, only a few percent of field galaxies is expected to lie within this narrow redshift range. In the two upper panels we show the E+S0 and S+I surface density as a function of radius, computed by removing the background as discussed above (Sec 6.1). Error bars are computed assuming Poisson statistics (Gehrels 1986) not corrected for field galaxy clustering. At large radii (the periphery) no statistically-significant excess of either type is found. This is due in part to the large additional uncertainties involved in the type-dependent subtraction. A small systematic over-subtraction of the background cannot be excluded, considering the cluster is optically-selected and the presence of a local background underdensity would have enhanced its discovery (Dressler 1984). The type-dependent excess is detectable out to a radius of 1 – 2 Mpc and becomes very significant only within the inner 1 Mpc. As far as the mix of morphological types is concerned, the densities of E+S0 and S+I galaxies remain quite similar down to the central regions and only within

the central 200 kpc does the E+S0 component become the dominant component.

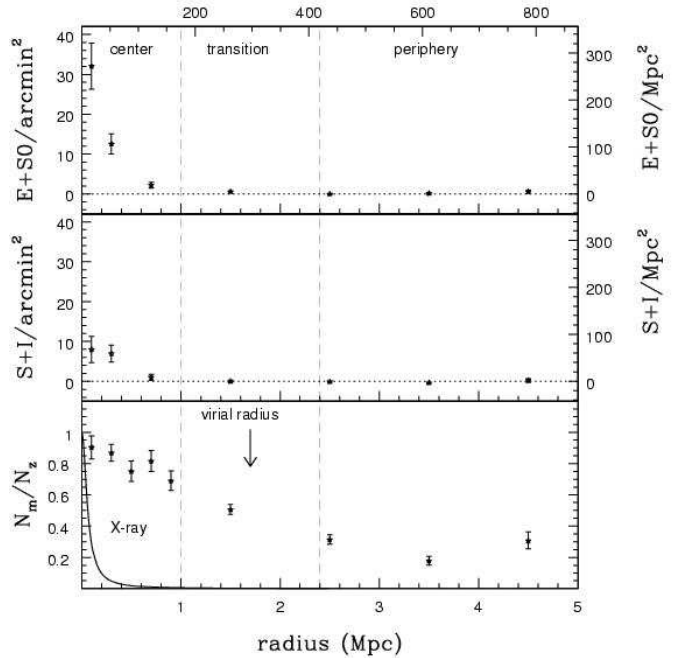


FIG. 12.— Radial trends. **Top panel:** Surface density of member E+S0 galaxies ($I < 21.1$) as a function of radius, after statistical removal of the background/foreground contamination. The density in galaxies per Mpc^2 is shown on the right scale for reference. Error bars assume Poisson statistics. **Middle panel:** as the top panel for spiral and irregular members. **Lower panel:** fraction of galaxies with redshifts (N_z) that are members (N_m) as a function of radius. Note that members are found to the outermost region probed. The three diagnostic regions defined in Section 5 and Figure 10 are indicated. The best fitting X-ray surface-brightness β profile (Böhlinger et al. 2001), in arbitrary units, is shown on the lower panels for comparison.

Figure 12 shows the importance of using spectroscopically confirmed members for the periphery. In the inner Mpc however, the error introduced by our statistical background/foreground correction is acceptable and both the WFPC2 and the WFPC2-z catalogs can be used. The result of enlarging the inner sample to include the WFPC2 catalog is shown in Figure 13 for both E+S0 (upper panel) and S+I (lower panel) galaxies. Fractions determined from the WFPC2-z sample are plotted as solid symbols, with errors determined assuming a binomial distribution. The fractions could be biased if the incompleteness depends on morphological types, which seems not to be the case (Sec 4.3). However, the numbers involved are small (~ 50 galaxies per radial bin) and the errors accordingly large. Fractions determined from the WFPC2 sample (open points) suffer less from small number statistics, therefore are probably to be preferred in the innermost regions ($\lesssim 0.5$ Mpc) when the uncertainty due to background/foreground contamination removal is sufficiently small.

The inner Mpc shows a steep gradient in morphological mix. E+S0 galaxies dominate and reach $\sim 75\%$ of the population in the inner 200 kpc (lower than in local clusters where they reach almost 100%, e.g. Whitmore, Gilmore & Jones 1993). Beyond 1 Mpc the fraction of E+S0 remains constant within the error, or at most mildly declining (from $51 \pm 7\%$ to $42 \pm 13\%$). A more signifi-

cant difference is seen between the morphological mix at 1 Mpc ($51 \pm 7\%$) and the field ($37 \pm 7\%$). The field fraction was determined by combining the subsample of the CFRS-LDSS with HST images (Brinchmann et al. 1998), limited to $I < 21.1$ and to $0.3 < z < 0.5$, interlopers located in the Cl0024+16 WFPC2-z catalog with $I < 21.1$, $0.3 < z < 0.37$ or $0.42 < z < 0.50$, and interlopers located in the Morphs database with HST images in F814W and $I < 21.1$, in the range $0.3 < z < 0.5$. These field samples are the most appropriate given that they were consistently classified by the same classifier (RSE), and are either spectroscopically complete (CFRS-LDSS) or at least suffer from similar incompleteness as the cluster samples (Cl0024+16 and the Morphs). However, the mix in the field sample is affected by small number statistics¹¹ and cosmic variance. Surprisingly, no larger spectroscopically complete sample of field galaxies with HST imaging is yet available to improve this comparison. The accuracy of the cluster fractions will improve when more redshifts in the periphery will be available, allowing us to improve the determination of the slope of the early-type fraction from the transition region to the periphery to the field.

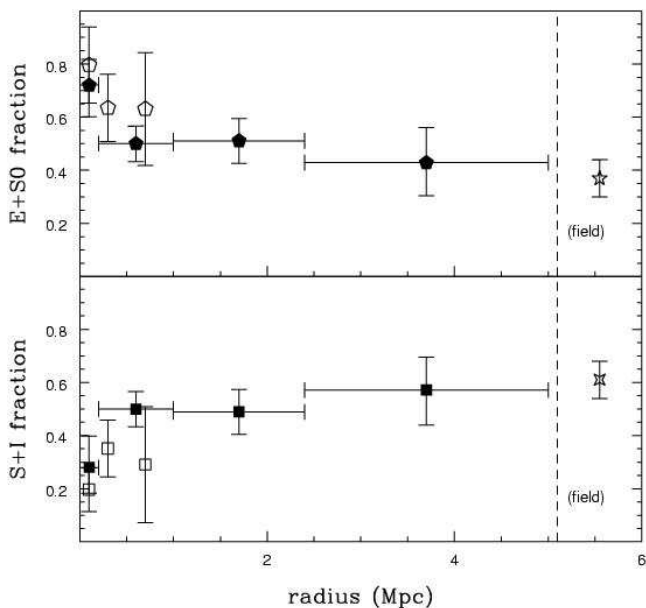


FIG. 13.— The fraction of morphological types ($I < 21.1$) in Cl0024+16 as a function of cluster radius: (upper panel) fraction of E+S0 galaxies; (lower panels) fraction of spirals. Fractions determined from the entire WFPC2 sample – removing the background statistically as detailed in Section 6.1 – are shown as large empty points, while fractions determined from the spectroscopic WFPC2-z catalog are shown as solid points. Points beyond the dashed line at 5.1 Mpc are field fractions determined from the CFRS-LDSS survey ($0.3 < z < 0.5$; Brinchmann et al. 1998), field galaxies in the Cl0024+16 area in the cluster vicinity ($0.3 < z < 0.37$ or $0.42 < z < 0.4$), and interlopers with F814W imaging from the Morphs collaboration (Smail et al. 1997; Dressler et al. 1999).

6.2.2. Discussion

As a first step in understanding the radial run of the E+S0 fraction, we seek to identify which physical mechanism(s) among the ones described in Section 5 can (or cannot) be responsible for the transformation of the in-

falling galaxies. To investigate this, we will consider the three diagnostic regions defined in Section 4 (Figure 10 and Figure 12): the center, transition, and periphery.

In the transition region, isolated infalling galaxies cannot have experienced tidal effects or ram pressure stripping more recently than 0.5-1 Gyr ago. In the periphery most of the galaxies *have never been through the center* and therefore are free from the effects of tidal stripping, tidal triggering of star formation and ram-pressure stripping. The mild decline in star formation associated with the gentle demise of spirals between the field and the transition region (Figure 13) cannot be ascribed to tidal interactions with the cluster potential nor to ram pressure stripping or triggering of star formation none of which are effective here. Setting aside merging – which we will discuss later – this leaves us starvation and harassment. Ultimately, a direct observation that the infalling population has smaller gas reservoirs than in the field would be needed to discriminate these. Accurate star formation diagnostics at large radii would provide some constraints. If significant numbers of starbursting/post-starburst galaxies (see Dressler et al. 1999; Poggianti et al. 1999) are found at the periphery, quenching would have to occur after a burst had depleted the gas, in contrast with the starvation picture (Balogh, Navarro, Morris 2001; Diaferio et al. 2001). Harassment should be detectable through an increased fraction of disturbed/interacting galaxies with respect to the field (Oemler et al. 1997). Unfortunately, it is not obvious how to unambiguously recognize the effects especially for high surface brightness Milky-Way type spirals where the signatures could be subtle (Moore et al. 1999).

Whichever mechanisms are involved, the timescales for the gradual morphological transformation between the field and the transition region are rather slow (see Section 5 and Appendix C). Are the same phenomena, appropriately accelerated and intensified, responsible also for the steep trend in the inner Mpc? Or are additional mechanisms at work? A quenching mechanism could produce gentle morphological changes over a few Gyr and the mild gradients observed beyond 1 Mpc radius. An additional mechanism, more appropriate to the cluster center, would induce rapid and dramatic changes via bursts of star formation and/or major structural changes. Multiple mechanisms/timescales have been discussed by Poggianti et al. (1999) and Dressler et al. (1999) who claim that the star formation properties of infalling galaxies react rapidly to environmental influences becoming visible as soon as they sense the cluster potential. By contrast, more time is needed for significant morphological transformations.

A completely different possibility discussed in the next section involves a segregation effect. Objects at different radii represent ones with different early assembly (merger) histories which are insufficiently mixed in the cluster to erase correlations between their history and their current location (Diaferio et al. 2001).

6.3. The morphology-density relation

6.3.1. Observations

We now examine the $T - \Sigma$ relation to further investigate the infalling scenario and the effects of segregation.

¹¹ The numbers are E+S0/S+I/Total 24/39/64 i.e. $37 \pm 7\%$, $61 \pm 7\%$, assuming binomial distribution.

Following Dressler (1980), we estimate the local projected density associated with each galaxy by computing the area of the rectangle with sides parallel to the cardinal axis that encloses the galaxy and its ten nearest neighbors, using this area to compute the local density, and finally by removing the background contamination (as described above in Section 6.1). We only consider those galaxies associated with a positive density.

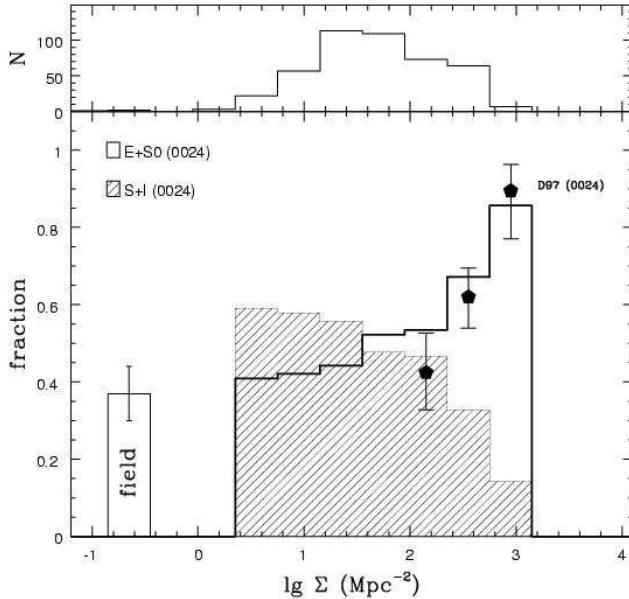


FIG. 14.— Morphology-projected density relation for galaxies in CL0024+16. For comparison, points with error bars show the fraction of E+S0 determined by the Morphs collaboration for the central field of CL0024+16 (Smail et al. 1997; Dressler et al. 1997). The histogram with error bar at low surface densities represents the fraction of E+S0 in the field at $z \sim 0.4$ (at $I < 21.1$; see Section 6.2 for discussion).

The resulting T- Σ relation (Figure 14) shows that the fraction of early-type galaxies increases monotonically with local surface density. For comparison, we overplot the fraction of E+S0 as a function of projected density for the central region of CL0024+16 as determined by the Morphs collaboration (Smail et al. 1997; Dressler et al. 1997)¹², as appropriate for our assumed cosmology and magnitude limit.

Our data extends the measurement by well over an order of magnitude in projected density Σ . In the region of overlap there is a good agreement between the two measurements. The slope in the fraction of E+S0 galaxies appears to flatten just below the limit probed by the Morphs, declining gently from $\sim 50\%$ towards the field¹³ value of $37 \pm 7\%$ (obtained as described in § 6.2). This behavior is very similar to that observed locally, where the T- Σ relation extends over several orders of magnitude in density from clusters continuously to the field (Postman & Geller 1984; see also Bhavsar 1981, de Souza et al. 1982, Giovanelli et al. 1986).

¹² A very similar relation is obtained by combining data from the three high-concentration clusters observed by the Morphs collaboration in the F814W filter, i. e. CL0024+16, CL0016+16, CL0054-27.

¹³ The surface density of the field has been estimated as the counts yielded by the galaxy luminosity function (e. g. Ellis et al. 1996) integrated 10 Mpc along the line of sight.

¹⁴ We also tried dividing the sample in two, inside and outside 0.5 Mpc, and the results are very similar to the case discussed here.

6.3.2. Discussion

The existence of the T- Σ relation at low densities was not *a priori* implied by the existence of the $T - R$ relation, even for an approximately regular cluster such as CL0024+16. Figure 15 shows that local density is not a well defined function of radius, except in the central ~ 0.5 Mpc. Spikes in projected density – such as that at ~ 1 Mpc – arise as a result of substructures (a similar phenomenon is seen also locally, see e.g. Andreon 1996).

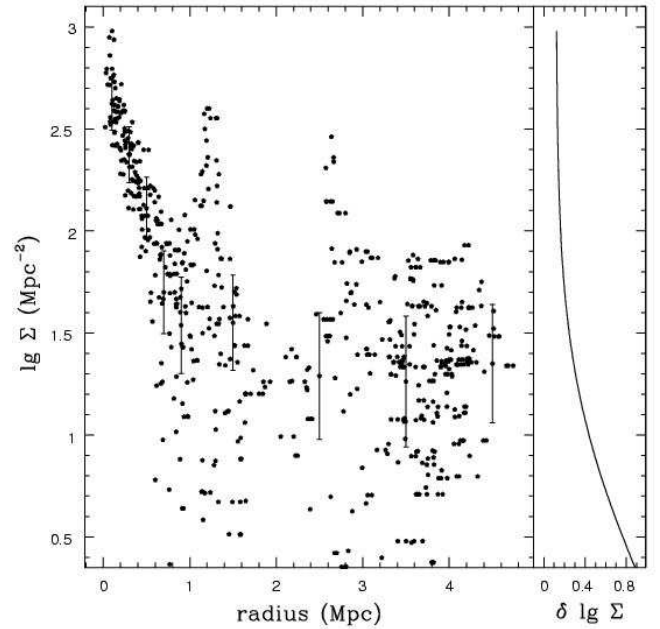


FIG. 15.— Local surface density vs cluster radius in CL0024+16 revealing the large range at a given radius and the spike in local density at ~ 1 Mpc. The points with error bars indicate the average Σ within radial bins, and the scatter expected from measurement errors, based on Poisson statistic for the cluster members and on the uncertainty on the background removal based on the two-point angular correlation function measured by Postman et al. (1998). The expected uncertainty as a function of Σ is shown in the right panel.

The scatter is significantly larger than expected from measurement errors. Using the definition of Σ (Dressler 1980), the measurement scatter can be estimated assuming a Poisson distribution for the cluster members and the field to field variation of the background, corrected using the two-point correlation function as measured by Postman et al. (1998). The expected error as a function of Σ is shown in the right panel of Figure 15, while the points with error bars represent the average Σ in radial annuli, with the scatter expected from measurement uncertainties.

How is the scatter in the local density at a given radius consistent with the derived T- Σ relation? At face value the existence of a relation implies galaxies are more aware of their local overdensity than cluster location. We investigated this further by dividing our sample in two subsets¹⁴: one from the central POS00 field (i.e the inner 0.5 Mpc, where the $\Sigma - R$ relation is monotonic) and one from the

overdensity ~ 1 Mpc NW of the center corresponding to the spike in local density in Figure 15 (POS36, see map in Figure 1).

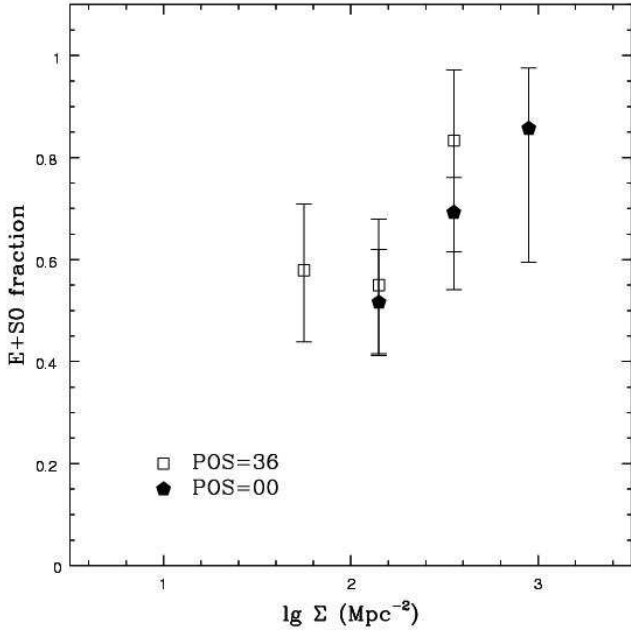


FIG. 16.— The fraction of E+S0 galaxies in Cl0024+16 as a function of local projected density for galaxies in the central (solid pentagons) and in the NW overdensity region (open squares; POS36) corresponding to the spike in local density at ~ 1 Mpc in Figure 15. Note the close match in the regions of overlapping density.

Figure 16 shows the results of this exercise. The fraction of early-type galaxies still correlates with the local density in the two subsets, i. e. galaxies at large radii clearly “know” if they are in a local overdensity. In the overlapping density region, the fractions of morphological types are mutually consistent. These conclusions are particularly significant when one considers that the cluster galaxies within ~ 1 Mpc are moving at speeds of ~ 1 Mpc Gyr $^{-1}$. At the typical densities of ~ 100 gal Mpc $^{-2}$ where differences in the morphological mix become significant, the smoothing box inherent to our measurement is of order ~ 0.1 Mpc 2 . Hence galaxies with uncorrelated velocity vectors would erase the T- Σ relation in much less than a Gyr, unless we assume that morphology is a transient phenomenon with implausibly short duration.

Not only are galaxy properties arranged according to their local environment but apparently in undertaking their motion within the cluster potential they *move with it* (i.e. they retain their identity in these groups as infall continues). This is a clear indication that – at least outside the central region – the cluster is more logically viewed as a collection of larger self-contained poorly-mixed clumps (Dressler & Shectman 1988, Zabludoff & Franx 1993). The presence of substructure is confirmed at high significance by the Dressler & Shectman (1988) test: even considering galaxies in peak A alone the probability of positions and radial velocities being uncorrelated is less than 4×10^{-4} ($< 10^{-4}$ combining peaks A and B). Another way to view this result is that, within the error bars, outside the cluster center, the mix of morphological types at given surface density is irrespective of that clump’s location within the cluster (see Figure 16).

Although radial trends in morphology were discussed in Section 6.2 in the context of infall timescales, we have argued on the basis of Figures 14-16, that outside 1 Mpc, the local projected density plays the main role. We interpret this as evidence that Cl0024+16 is accreting galaxies in organized substructures, each of which obeys some form of T- Σ relation. An interesting explanation of our observations would be that the correlation between local density and morphology arises as a result of pre-cluster conditions, possibly because galaxies located at different local densities suffered different assembly and star formation histories.

Both radial and density effects are important but influence different regimes. Beyond $\sim 0.5 - 1$ Mpc, we are witnessing trends that relate to the previous assembly histories of infalling groups. Starvation may play some role in changing the fate of galaxies in these clumps, but whatever process is at work, it operates slowly and is insufficient to supplant that based on segregation which is not erased by mixing. Inwards of $0.5 - 1$ Mpc, the tight correlation between radius and density (Figure 15) presumably follows the disruption of this substructure. At this level, the correlation with the initial local environment is probably lost, while retaining the morphological segregation as a function of radius. The cluster radius then becomes the fundamental variable. Phenomena more closely related to the cluster potential – such as tidal interaction or ram pressure stripping – may play an additional role in morphological transformations.

The T- Σ trend found outside the central region strengthens our earlier conclusion (Section 6.2.2) that ram-pressure stripping, ram-pressure triggering of star formation, tidal truncation and tidal-triggering of star formation by the main cluster potential are not dominant. Further a T- Σ relation is also found locally in non-concentrated systems, where presumably the effects of the overall cluster potential and the ICM are negligible; Dressler 1980).

Finally, Figure 17 compares our T- Σ relation for Cl0024+16 with that determined locally (Dressler 1980, revised in Dressler et al. 1997). At projected densities higher than ~ 20 gal Mpc $^{-2}$, the fraction of early-type galaxies is higher in the local Universe than in Cl0024+16 at any given Σ . This agrees with other intermediate redshift studies which indicate that the fraction of E+S0 declines with redshift (e. g. van Dokkum et al. 2001). An equally interesting result (unique to the Cl0024+16 dataset) is that at local densities below ~ 20 gal Mpc $^{-2}$ the morphological mix at $z \approx 0.4$ is indistinguishable (within the errors) to that observed locally. A related result is seen in the T-R relation at the periphery (c.f. Figure 13 with Figure 12 in Dressler et al. 1997). The field number densities are insufficiently precise to establish whether this is a displacement of E+S0 galaxies from the field to the highest density regions, a transformation of spirals into E+S0s, or a combination. Regardless, it is clear that the morphological mix of galaxies in low density environments has not changed significantly since $z \sim 0.4$ (~ 30 % of the Hubble time). In combination with the (at most) mild gradients of morphological fraction at large radii discussed in Section 6.2.2, and with the mild decline in star formation rate in the outer parts of clusters, we interpret this as further evidence that slow environmental processes are at

work in the outer parts of clusters.

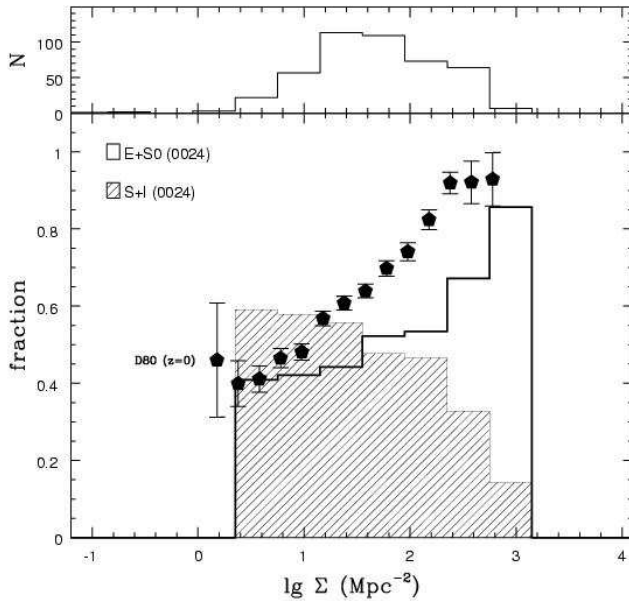


FIG. 17.— The morphology-projected density relation for galaxies in CL0024+16 (histogram) compared to the local relation as determined by Dressler et al. (1997). The local early-type fraction is shown as red solid pentagons (for clarity the spiral fraction is omitted). The local relation has been corrected to our adopted value of the Hubble constant $H_0 = 65 \text{ km s}^{-1} \text{ Mpc}^{-1}$.

7. CONCLUSIONS

In this paper we have presented the first results from a wide field HST survey of the rich galaxy cluster CL0024+16 at $z \approx 0.4$. We exploit an unique wide-field mosaic of HST WFPC2 images and relate these to available spectroscopic data in order to examine the morphological mix as a function of radius and projected galaxian density. Our main observational results can be summarized as follows:

1. We have obtained WFPC2 observations (39 independent pointings) covering an approximately circular region of 10 Mpc in diameter around the center of CL0024+16. The areal sampling ranges from 100 % at the center to $\sim 20\text{-}40$ % at the periphery. We produce an object catalog comprising over 22,000 objects to $I \sim 25$ (F814W). All 2200 objects to $I = 22.5$ have been morphologically classified in a scheme broadly similar to that adopted for the Medium Deep Survey.
2. Approximately 100 new redshifts in the field have been obtained using the W. M. Keck I telescope. Together with other redshift catalogs (Dressler et al. 1999; Czoske et al. 2001; Owen 2001; Metevier & Koo 2001) this brings the total number of objects with redshift to 787 (including 358 members; $0.374 < z < 0.402$). After cross correlation with the morphological WFPC2 catalog we created the redshift WFPC2-z catalog, consisting of 362 objects with both redshift and WFPC2 imaging (195 cluster members).
3. Using a simple model for the cluster based on the observed mass estimate and X-ray surface brightness profile (Appendix A), we have estimated the time and velocity scales for galaxy infall and the regions of influence of various mechanisms proposed to account for environment evolution. We define three projected regions; the cluster center ($\lesssim 1$ Mpc) where tidal effects of the cluster potential and those of the ICM are dominant; the transition region ($\sim 1\text{-}2.4$ Mpc, comprising the virial radius) where galaxies do not experience the strong interaction with the cluster potential and the ICM, but some fraction of galaxies may have experienced interaction with the cluster center in the recent past (< 1 Gyr), and the periphery beyond 2.4 Mpc where galaxies are entering the cluster for the first time and where environmental trends are driven by slow (> 1 Gyr) phenomena.
4. We have used the morphological catalog (WFPC2) and the redshift catalog (WFPC2-z) to study the galaxy population and the mix of morphological types with cluster radius (the so-called $T - R$ relation) to the previously unexplored regions beyond 1 Mpc at $z=0.4$. Cluster galaxies ($0.374 < z < 0.402$) are found out to 5 Mpc from the cluster center, but the marginal excess with respect to the background makes precise studies difficult until further spectroscopy is available. The fraction of members declines from $>60\text{-}70\%$ in the center, to $\sim 40\%$ in the transition region, and less than $\sim 20\%$ at the periphery. Consistent with previous investigations, the fraction of E+S0 galaxies ($I < 21.1$) is highest ($73 \pm 10\%$) in the central core within 200 kpc from the center and declines rapidly to ~ 50 % at 1 Mpc. It then changes very mildly over the next 4 Mpc reaching a value (43 ± 13 %) at the periphery indistinguishable from the field (37 ± 7 %). The most significant changes in the $T - R$ relation occur within a radius of 1 Mpc.
5. We also studied the run of morphological mix with local projected density (the so-called $T - \Sigma$ relation). At intermediate redshift we extend this relation by over an order of magnitude in Σ over previous determinations (Dressler et al. 1997). The fraction of E+S0 galaxies falls rapidly over the densest decade and then flattens out at $\Sigma \sim 10$ gal Mpc^{-2} at $\sim 45\%$, slightly above the field value. Outside the central ~ 0.5 Mpc we find a large scatter in values of Σ at given radius, with overdensity peaks associated with identifiable clumps in the two-dimensional galaxy distribution. Overdensities at large cluster radii have the same mix of morphological types as the similar ones at small cluster radii. Remarkably, in the region of overlapping densities the $T - \Sigma$ relation of these inner and outer regions are identical. In comparison to local samples, CL0024 has a smaller fraction of E+S0 galaxies at densities above ~ 20 gal Mpc^{-2} (in agreement with previous studies), while at densities below this limit the fraction of E+S0 is unchanged within the uncertainties.

Although we are continuing to gather spectroscopic data, we interpret our current results as follows. The mild gradients found at large radii in the morphological mix cannot be explained by mechanisms such as tidal triggering of star formation and tidal stripping of the dark matter halos by the main cluster potential, nor by ram pressure triggering of star formation, or ram pressure stripping, which are ineffective in these regions. Instead we suggest that other mechanisms such as starvation or harassment operate over timescales of several Gyrs. Starvation seems a promising candidate to explain the mild trends in the morphological mix, since it would explain also the mild gradients in the star formation rate seen by Abraham et al. (1996b; see also Balogh et al. 1999 and Balogh, Navarro & Morris 2000).

A gradual mechanism would also explain the homogeneity of the early-type galaxy population located in the cluster centers (Bower, Lucey & Ellis 1992; Ellis et al. 1997; Stanford, Eisenhardt & Dickinson 1998; van Dokkum et al. 1998b; Kelson et al. 2000), and the small differences observed between their clustered and field populations at various redshifts (Bernardi et al. 1998; Treu et al. 1999, 2001b, 2002; Kochanek et al. 2000; van Dokkum et al. 2001). The homogeneity might be understood if the quenching of star formation occurred gradually rather than via a series of discrete events. Secondary bursts of star formation can be reconciled with the homogeneity of the stellar populations in local and distant E+S0 galaxies (e.g. Bower, Kodama & Terlevich 1998; Treu et al. 2001b) and with the detection of post-starburst K+A galaxies in clusters (Poggianti et al. 1999). However, if the mass distribution was also altered – as during harassment – significant fine-tuning of the star formation and structural changes would be needed to preserve the tight scaling laws. High quality spectroscopic data, secured as a function of cluster radius, will address these issues and help to identify the mechanisms at work. Such data will also help clarify the origin of the sharp rise in the E+S0 fraction in the core.

A more attractive (not necessarily alternative) possibility is that the T-R relation is mostly due to segregation,

following an inbuilt correlation between galaxy properties and their local substructures. This is supported by a convincing T- Σ relation outside the central region where Σ and radius show a large scatter. In order for the T- Σ relation to be sustained outside the central concentration, not only must such correlations be defined within each subclump, but also the galaxies contained within them must be moving coherently. Although a more detailed physical picture must await further dynamical data in the cluster outskirts, we present an emerging picture where the assembly and star formation of individual subclumps falling into the cluster (see also Kodama et al. 2001) dominates the morphological trends outwards of $\sim 0.5 - 1$ Mpc.

We are grateful to Frazier Owen, Anne Metevier, and David Koo for sharing their lists of redshifts with us in advance of publication. We thank Judy Cohen and Patrick Shopbell for writing and supporting the software AUTOSLIT that we used to design the LRIS masks. TT acknowledges useful conversations with Andrew Benson, Kevin Bundy, Chris Conselice, Bianca Poggianti, David Sand, Pranjal Trivedi, Pieter van Dokkum. The referee is thanked for comments that helped clarifying the presentation of the results. Finally, the authors wish to recognize and acknowledge the cultural role and reverence that the summit of Mauna Kea has always had within the indigenous Hawaiian community. We are most fortunate to have the opportunity to conduct observations from this mountain.

This paper is based on observations collected at the W. M. Keck Observatory, which is operated jointly by the California Institute of Technology and the University of California, and with the NASA/ESA Hubble Space Telescope, obtained at the Space Telescope Science Institute, which is operated by AURA, under NASA contract NAS5-26555. We acknowledge financial support for proposal number HST-GO-8559 provided by NASA through a grant from STScI, which is operated by AURA, under NASA contract NAS5-26555. Ian Smail acknowledges support from the Royal Society and the Leverhulme Trust.

APPENDIX

A SIMPLE CLUSTER MODEL

In this appendix we consider a very simple model for a galaxy infalling radially onto the cluster. This model will be later used to estimate the relevant spheres of influence of physical mechanisms operating in Cl0024+16 and the infalling timescales.

First, we need to compute the *virial radius* r_V which contains the virialized mass (Gunn & Gott 1972). This can be obtained in terms of the galaxy velocity dispersion at large radii (σ_∞) as

$$r_V = 1.7 h^{-1} \text{Mpc} \left(\frac{\sigma_\infty}{1000 \text{ km s}^{-1}} \right) [\Omega_m(1+z)^3 + \Omega_\Lambda]^{-1/2} \quad (\text{A1})$$

in a flat cosmology (Carlberg, Yee, Ellingson 1997; Girardi & Mezzetti 2001), i.e. ~ 2 Mpc adopting $\sigma_\infty = 911 \text{ km s}^{-1}$ (Girardi & Mezzetti 2001) with our choice of the cosmological parameters. For Cl0024+16, the velocity dispersion is affected by the presence of a secondary peak in the distribution suggestive of an infalling group (Czoske et al. 2002). At large radii the velocity dispersion of primary peak flattens at $\sim 600 \text{ km s}^{-1}$, and this can be considered a lower limit to σ_∞ , hence $r_V \gtrsim 1.3$ Mpc. For the present analysis, we will consider the indicative value of the virial radius to be approximately $r_V \sim 1.7$ Mpc.

For simplicity, we assume the cluster mass density scales as $\rho \propto r^{-2}$ inside the r_V and is zero outside. The absolute normalization is obtained using the values given by Soucail et al. 2001 (we consider the average of X-ray and strong lensing normalization, with a factor of two uncertainty). A radially infalling galaxy starting with zero velocity at turnaround

radius r_a hits the cluster at r_V with velocity V_V , as given by energy conservation

$$V_V = \sqrt{\frac{2GM_V}{r_V} - \frac{2GM_V}{r_a}}, \quad (\text{A2})$$

where G is the gravitational constant and M_V is the virial mass. For simplicity we take $r_a/r_V = 2$ (the uncertainty is dominated by other factors, such as mass uncertainty, using 1.5, 3 or 4 would not alter significantly the picture; for a more realistic description of the orbital properties of the infalling population see, e.g., Vitvitska et al. 2002), obtaining

$$V_V = \sqrt{\frac{GM_V}{r_V}}. \quad (\text{A3})$$

Using $M_V = 8 \cdot 10^{14} M_\odot$ and $r_V = 1.7$ Mpc, we obtain $V_V = 1400 \text{ km s}^{-1}$.

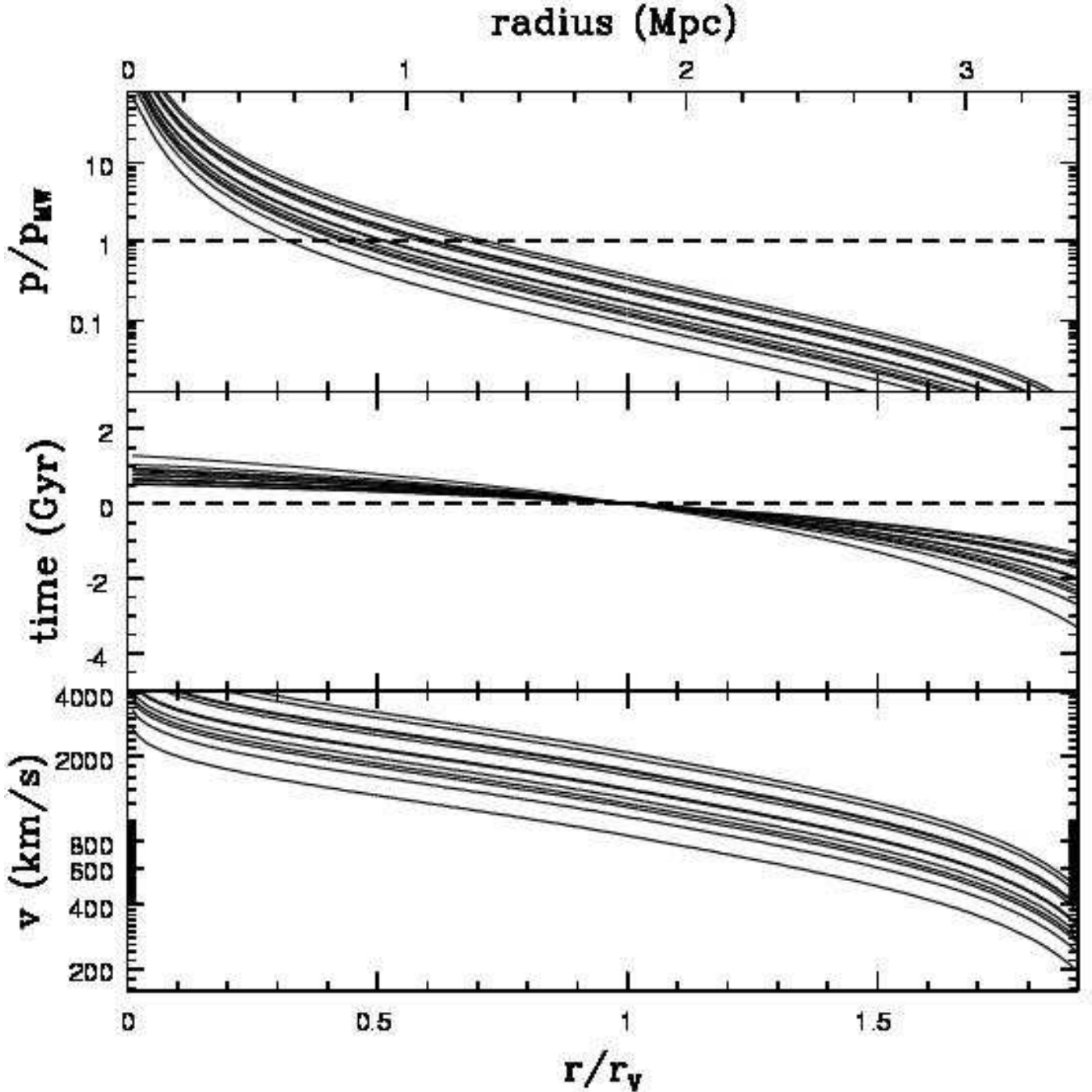


FIG. A18.— A radially infalling galaxy. Lower panel: velocity of a radially infalling galaxy computed using a static isothermal model for the mass distribution of cluster CL0024+16. Middle panel: travel time from the virial radius. Upper panel, ram pressure in units of the ram pressure needed to strip a galaxy like the Milky-Way of its gas. The various lines are obtained for different values of the cluster mass normalization (Soucail et al. 2000), and of the ratio between turnaround radius and virial radius $r_{ta}/r_V = 1.5, 2, 3, 4$.

The infalling velocity $v_i(r)$ and time $t_i(r)$ as a function of radius are then found solving the equation of motion, providing a rough estimate of the motion of infalling galaxies (see Fig A18). The travel time between the center and the virial radius is ~ 1 Gyr, while 2-4 Gyr are needed to travel between the r_V and $2r_V$ (depending on mass normalization and on r_a/r_V). These travel times imply average velocities of order 2000 km s^{-1} between the center and r_V and of order $500 - 1000 \text{ km s}^{-1}$ between r_V and $2r_V$. In general, we expect a continuous distribution of orbital parameters for the infalling galaxies with only a small fraction of galaxies to be on highly eccentric or quasi-radial orbits (for example Ghigna et al. 1998 found that $\sim 20\%$ of the galaxies will pass in the central 200 kpc, i.e. $\sim r_V/10$). Hence we can assume that the travel times estimated with radial infalling galaxies are approximately a lower limit to the travel times of the population.

LENGTH SCALES

The first important quantity is the *stripping radius* r_{st} defined as that where a radially infalling galaxy with the properties of the Milky Way would have its gas removed by ram-pressure. We can estimate the stripping radius by considering the cluster mass model introduced in A together with the properties of the inter cluster medium. The gas density profile inside r_V is modeled with a β profile

$$\rho_{gas} = \rho_0 \left[1 + \left(\frac{r}{r_c} \right)^2 \right]^{-\frac{3}{2}\beta}, \quad (\text{B1})$$

with $\beta = 0.475$, $r_c = 60 \text{ kpc}$ and $\rho_0 = 3 \cdot 10^{14} M_\odot \text{Mpc}^{-3}$ (Böhlinger et al. 2001). Assuming the X-ray emitting gas is at rest with respect to the cluster, we can directly compute the ram pressure $p = \rho_{gas} v_i^2$ and check where ram pressure stripping is effective using the condition (Gunn & Gott 1972; see also Abadi, Moore & Bower 1999, Fujita & Nagashima 1999; Fujita 2001; Toniazzo & Schindler 2001)

$$\rho_{gas} v_i^2 > 2.1 \cdot 10^{-12} \text{Nm}^{-2} \left(\frac{v_{rot}}{220 \text{kms}^{-1}} \right)^2 \left(\frac{r_h}{10 \text{kpc}} \right)^{-1} \left(\frac{\Sigma_{HI}}{8 \cdot 10^{20} m_H \text{cm}^{-2}} \right), \quad (\text{B2})$$

where the rotational velocity of the infalling galaxy v_{rot} , its scale length (r_h), and surface density of HI (Σ_{HI}), are expressed in units appropriate for the Milky-Way (Spitzer 1978; Binney & Tremaine 1987). For an infalling Milky-Way the stripping radius occurs in the range $r_{st} = 0.5 - 1 \text{ Mpc}$, therefore we will assume $r_{st} \sim 0.75 \text{ Mpc}$. A similar estimate is obtained by considering that – given central velocity dispersion of the cluster galaxies $\sim 1000 \text{ km s}^{-1}$ (Soucail et al. 2001) – galaxies in the center of the cluster will have maximal velocity with respect to the X-ray emitting gas of order $\sim 2000 \text{ km s}^{-1}$. Using the gas density given in Equation B1 and the condition in Equation B2, we obtain a stripping radius $\sim 0.8 \text{ Mpc}$. Note that we are considering here the most favorable conditions for ram pressure stripping (i.e. maximal velocity) so that r_{st} is practically the maximal radius at which we expect to ram-pressure stripping to be effective. In summary, we estimate that for Cl0024+16 $r_{st} = 0.5 - 1 \text{ Mpc}$ at most.

Alternate mechanisms (thermal evaporation, viscous and turbulent stripping) might be more effective in this respect, depending on the detailed physics and the galactic orbits. For simplicity, we will assume that alternate mechanisms occur at most with the same intensity and therefore do not affect our estimate of the region where stripping is important.

The extended gas reservoir that may surround field galaxies (see Benson et al. 2000), sustains star formation in low density environments and is more loosely bound. Accordingly it can be removed at radii beyond r_{st} . This effect is dependent on the detailed physics, the galaxy orientation and the structure of the diffuse reservoir. We will assume that such starvation can be also effective at least to the virial radius (e. g. Abadi et al. 1999; Balogh et al. 2000).

Interactions with the ICM can also trigger star formation by increasing pressure on the ISM. However, according to Fujita (1998) and Fujita & Nagashima (1999), this mechanism seems to be negligible compared with tidally-induced pressure or harassment-induced pressure that we describe below.

Tidal interactions with the cluster potential affect galaxies in several ways. The effectiveness of tidal compression in triggering star formation depends on the cluster mass distribution, but detailed calculations (Byrd & Valtonen 1990; Herinksen & Byrd 1996; Fujita 1998) show that for clusters of mass comparable to Cl0024+16 the process is only effective within the central $\sim 200 \text{ kpc}$ at most. Tidal stripping (Merritt 1983, 1984) removes mass from the outer regions of a galaxy (typically at radii larger than the luminous component), thus altering the mass and cross sections for galaxy-galaxy interactions. Modeling the cluster and galaxy halos as isothermal spheres with velocity dispersions σ_c and σ_h (Moore et al. 1996, 1998) we derive the following estimate for the *cluster tidal truncation radius* r_{tt}

$$r_{tt} \geq \frac{\sigma_c}{\sigma_h} \sim r_o \left(\frac{\sigma_h}{1000 \text{ km s}^{-1}} \right)^{-1}, \quad (\text{B3})$$

limiting the cluster region where tidal truncation is important for the luminous component of the galaxies inside their optical radius r_o .

Less dense galaxies will be disrupted first, but typically only in the innermost regions (100-200 kpc; Moore et al. 1998). Removal of the diffuse gas reservoir will also be dominated by hydrodynamical effects and therefore we will neglect this mechanism in the estimation of regions where starvation is important.

Finally, we consider galaxy-galaxy interactions. Harassment (Moore et al. 1996) arises from an interplay between the overall cluster potential – which is responsible for tidal truncation of halos and the high speed of galaxies – and the local density – which affects the interaction rate. Schematically, the harassment rate f_H scales with the luminous galaxy density ρ_{gal} and mass m_{gal} as

$$f_H \propto \rho_{gal} m_{gal}^2 \propto \rho_{gal} r^2, \quad (\text{B4})$$

where we assume that galaxy masses are tidally truncated by the cluster potential. In the simple case where local density scales smoothly as r^{-2} – the harassment rate should be independent on cluster radius, within the validity limits of Equation B4 (Moore et al. 1998). In practice, there is spread in local density at a given radius (see Section 6), and therefore the rate depends somewhat on both variables. Note the effects of harassment on the morphology of a galaxy depend not only on its mass, but also on its internal structure. For example, typical L_* spirals in CL0024+16 could be transformed either into dwarf spheroidals or into lenticulars depending on the concentration of the mass distribution and on the disk scale length (Moore et al. 1999).

The merger frequency is a strong function of cluster radius, since it increases with density but decreases with velocity dispersion. Schematically, the rate peaks around the virial radius of the cluster and declines towards the center (see e.g. Ghigna et al. 1998). In hierarchical clustering, galaxies located at any given time at the cluster center are those that formed earlier and had the highest probability of having undergone major mergers in their past (Springel et al. 2001; Diaferio et al. 2001). This distinction emphasizes the difference between regions where phenomena happen from the regions where their effects are observed, as discussed in Section 5.2.

The regions of the cluster where the above physical processes are most effective are summarized in the upper panel of Figure 10.

TEMPORAL AND VELOCITY SCALES

To interpret the observed distribution of galaxies across a wide range of cluster radius we also need to consider the time scales involved and thus, by implication, the galaxy motions.

First, we estimate the time scales associated with the motions of galaxies in the cluster potential. As described in Appendix A, for a galaxy on a radial orbit, approximately¹⁵, ~ 1 Gyr is needed to traverse from the center to the virial radius, and $\sim 2-4$ Gyrs to travel between r_V and $2r_V$. As galaxies are not on purely radial orbits (e. g. Ghigna et al. 1998; van der Marel et al. 2000; Vitviska et al. 2002), a significant fraction of galaxies at or beyond the virial radius will never reach the cluster center. Hence these travel times can be considered lower limits. For motions in any given direction, the relevant velocity scale is given by $\sqrt{2GM_V/r_V}$ (where M_V is the virial mass, see Appendix A), corresponding to velocities of order ~ 1 Mpc Gyr⁻¹.

Second, a time scale can be associated with each of the *physical mechanisms* listed in Section 5.1. Starting with interactions between galaxies and the ICM, ram pressure stripping in the highest density ICM regions happens on a very short time scale ($\sim 5 \times 10^7$ yr; Abadi et al. 1999), while starvation according to our definition occurs more slowly, lasting up to several Gyrs. Galaxy-cluster gravitational interactions and tidal compression of gas clouds occur rapidly ($\sim 10^8$ yr), while tidal truncation occurs on time scales longer than the cluster crossing time, i.e. a few Gyr. Harassment transforms the morphology and star formation properties on timescales of a few Gyrs (e.g. Moore et al. 1999) while mergers can take place on time scales of a fraction of a Gyr and their morphological remnants would be undetectable after a few 10^8 yr (e. g. Mihos 1995).

Third, we can consider the timescales for witnessing changes in the star formation properties of a system. After a burst of star formation, massive stars are dominant at most during the initial $\sim 10^8$ yr while signatures such as strong Balmer emission lines such be detectable for ~ 1 Gyr after the burst (as k+a/a+k if the burst happened on top of a older stellar population; Dressler & Gunn 1983; Poggianti et al. 1999). The exact value depends not only on the prior and current star formation details but also on the actual observable (e.g. Barger et al. 1996). However, for simplicity in this paper we will adopt a typical time of ~ 1 Gyr for alteration in the colors and luminosity of a galaxy after a burst.

Finally, the timescale associated with starvation is linked to that for gas consumption due to star formation. Larson et al. (1980) estimate that it takes a few Gyrs for a typical Milky Way Galaxy to run out of gas, and cease star formation. Thereafter, they show that the optical colors change slowly after the next few Gyrs (see also Abraham et al. 1996b).

REFERENCES

- Abadi, M. G., Moore, B., Bower, R. G. 1999, MNRAS, 308
 Abraham, R. G., van den Bergh, S., Glazebrook, K., Ellis, R.S.,
 Santiago, B. X., Surma, P., Griffiths, R., E. 1996a, ApJS, 107, 1
 Abraham, R. G. et al. 1996b, ApJ, 471, 694
 Andreon, S. 1996, A&A, 314, 763
 Andreon, S. 1998, ApJ, 501, 533
 Bacon, D., Refregier, A., Ellis, R.S. 2000, MNRAS, 318, 625
 Balogh, M. L., Morris, S. L., Yee, H. K. C., Carlberg, R. G.,
 Ellingson, E. 1999, ApJ, 527, 54
 Balogh, M. L., Navarro, J. F., Morris, S. L. 2000, ApJ, 540, 113
 Balogh, M. L. et al. 2002, ApJ, 566, 123
 Barger, A. J., Aragon-Salamanca, A., Ellis, R. S., Couch, W. J.,
 Smail, I., Sharples, R. M. 1996, MNRAS, 279, 1
 Bekki, K. 1998, ApJ, 502, L133
 Bernardi M., Renzini A., da Costa L. N., Wegner G., Alonso M. V.,
 Pellegrini P.S., Rit e C., Wilmer C. N. A., 1998, ApJ, 508, L43
 Bernardi, M. et al. 2003, AJ, in press, astro-ph/0301626
 Bertin, E. & Arnouts, S. 1996, A&AS, 117, 393
 Benson, A.J., Bower, R.G., Frenk, C.S., White S. D. M. 2000,
 MNRAS, 314, 557
 Bhavsar, S. P., 1981, ApJ, 246, L5
 Bower, R. G., Lucey, J. R. & Ellis, R.S., 1992, MNRAS, 254, 601
 Bower, R. G., Kodama, T., & Terlevich, A. 1998, MNRAS, 299, 1193
 B ohringer, H., Soucail, G., Mellier, Y., Ikebe, Y., Schuecker, P. 2000,
 A&A, 353, 124
 Brinchmann, J. et al. 1998, ApJ, 499, 112
 Broadhurst, T., Huang, X., Frye, B., Ellis, R.S. 2000, ApJ, 534, L1
 Bruzual A. G., Charlot S., 1993, ApJ, 405, 538
 Butcher, H. & Oemler, A. 1978, ApJ, 219, 18
 Butcher, H. & Oemler, A. 1984, ApJ, 285, 426
 Byrd, G., Valtonen, M. 1990, ApJ, 350, 89
 Caldwell, N. 1984, PASP, 96, 287
 Carlberg, R.G., Yee, H.K.C., Ellingson, E. 1997, ApJ, 478, 462
 Casertano, S. et al. 2000, AJ, 120, 2747
 Cohen, J. G., Hogg, D. W., Blanford, R. G., Cowie, L. L., Hu, E.,
 Songaila, A., Shoppell, P. & Richberg, K. 2000, ApJ, 538, 29

¹⁵ Note that this simple model assumes a fixed cluster potential, so it is clearly not appropriate for timescales of several Gyrs, where we expect the cluster to evolve significantly, and therefore should only be regarded as indicative.

- Couch, W. J., Ellis, R. S., Sharples R. M. & Smail, I. 1994, *ApJ*, 430, 121
- Couch, W. J., Barger, A. J., Smail, I., Ellis, R. S., Sharples, R. M., 1998, *ApJ*, 497, 188
- Cowie, L. L., Songaila, A. 1977, *Nature*, 266, 501
- Czoske, O., Kneib, J.-P., Soucail, G., Bridges, T., Mellier, Y., Cuillandre, J.-C., 2001, *A&A*, 372, 391
- Czoske, O., Moore, B., Kneib, J.-P., Soucail, G., 2002, *A&A*, 386, 31
- Diaferio, A., Kauffmann, G., Balogh, M. L., White, S. D. M., Schade, D., Ellingson, E. 2001, *MNRAS*, 323, 999
- Djorgovski S. G. & Davis M. 1987, *ApJ*, 313, 59
- Drake, N., Merrifield, M.R., Sakelliou, I., Pinkney, J.C., 2000, *MNRAS*, 314, 768
- Dressler, A. 1980, *ApJ*, 236, 351
- Dressler, A. 1984, *ARA&A*, 22, 185
- Dressler, A., Gunn J. E. 1983, *ApJ*, 270, 7
- Dressler, A., Gunn J. E. 1992, *ApJS*, 78, 1
- Dressler, A. & Shectman, S. 1988, *ApJ*
- Dressler, A., Lynden-Bell, D., Burstein, D., Davies, R. L., Faber, S. M., Terlevich, R., Wegner G. 1987, *ApJ*, 313, 42
- Dressler A., Oemler A., Butcher H. R. & Gunn, J.E. 1994, *ApJ*, 430, 107
- Dressler A., et al. 1997, *ApJ*, 490, 577
- Dressler A., Smail I., Poggianti, B., Butcher, H., Couch W. J., Ellis R. S., Oemler A. 1999, *ApJS*, 122, 51
- Dye, S., Taylor, A. N., Greve, T.R., Rönvaldsson, Ö.E., van Kampen, E., Jakobsson, P., Sigmundsson, V.S., Gudmundsson, E.H., Hjorth, J. 2002, *A&A*, 386, 12
- Ellis, R.S., Colless, M., Broadhurst, T.J., Heyl, J.S., & Glazebrook, K., 1996, *MNRAS*, 280, 235
- Ellis, R.S., Smail I., Dressler, A., Couch, W. J., Oemler, A., Butcher, H., Sharples, R. M., 1997, *ApJ*, 483, 582
- Evrard, A. E. 1991, *MNRAS*, 248, 8
- Fabricant, D., Franx, M., van Dokkum, P.G., 2000, *ApJ*, 539, 577
- Fisher, D., Fabricant, D., Franx, M., van Dokkum, P. G. 1998, *ApJ*, 498, 195
- Fort, B., Mellier, Y., Dantel-Fort, M. 1997, *A&A*, 321, 353
- Fruchter, A. S. & Mutchler, M. 1998, <http://www-int.stsci.edu/fruchter/dither/ditherII.ps>
- Fruchter, A. S. & Hook, R. N. 2002, *PASP*, 114, 144
- Fujita, Y. 1998, *ApJ*, 509, 587
- Fujita, Y. 2001, *ApJ*, 550, 612
- Fujita, Y., Nagashima, M. 1999, *ApJ*, 516, 619
- Gehrels, N. 1986, *ApJ*, 303, 336
- Ghigna, S., Moore, B., Governato, F., Lake, G., Quinn, T., Stadel, J., 1998, *MNRAS*, 300, 146
- Giovanelli, R. G., Haynes, M. P. & Chincarini, G. L., 1986, *ApJ*, 300, 77
- Girardi, M. & Mezzetti M. 2001, *ApJ*, 548, 79
- Glazebrook, K., Ellis, R., Santiago, B. & Griffiths, R. E. 1995, *MNRAS*, 275, L19
- Griffiths E. et al. 1994, *ApJ*, 435, L19
- Gunn, J. E., Gott, R. J. 1972, *ApJ*, 176, 1
- Icke, V. 1986, *A&A*, 144, 115
- Henriksen, M. J. & Byrd, G., 1996, *ApJ*, 459, 82
- Kauffmann, G. 1995a, *MNRAS*, 274, 153
- Kauffmann, G. 1995b, *MNRAS*, 274, 161
- Kauffmann, G. 1996, *MNRAS*, 281, 478
- Kelson D. D., Illingworth G. D., van Dokkum, P. G. & Franx, M. 2000, *ApJ*, 531, 184
- Kochanek, C. S. et al. 2000, *ApJ*, 543, 131
- Kodama, T. & Smail, I. 2001, *MNRAS*, 326, 637
- Kodama, T., Smail, I., Nakata, R., Okamura, S. & Bower, R. G. 2001, *ApJ*, 562, L9
- Larson, R. B., Tinsley, B. M., Caldwell, C. N., 1980, *ApJ*, 237, 692
- Lilly, S. J., Le Fevre, O., Crampton, D., Hammer F., Tresse, L. 1995, *ApJ*, 455, 50
- Lilly, S. J. et al. 1998, *ApJ*, 500, 75
- Melnick, J., Sargent W.L.W. 1977, *ApJ*, 215, 401
- Metevier A. J., Koo D. & Simard, L. 2001 to appear in "Tracing Cosmic Evolution with Galaxy Clusters", Borgani, Mezzetti & Valdarnini eds. *astro-ph/0110194*
- Merritt, D. 1983, *ApJ*, 264, 24
- Merritt, D. 1984, *ApJ*, 276, 26
- Mihos, C. 1995, 438, L75
- Moore, B., Lake, G., Katz, N. 1998, *ApJ*, 495, 139
- Moore, B., Katz, N., Lake, G. 1996, *ApJ*, 457, 455
- Moore, B., Katz, N., Lake, G., Dressler, A., Oemler A. 1996, *Nature*, 379, 613
- Moore, B., Lake, G., Quinn, T., Stadel, J., 1999, *MNRAS*, 304, 465
- Natarajan, P., Kneib, J.-P., Smail, I., Ellis, R.S. 1998, *ApJ*, 499, 600
- Nulsen, P. E. J. 1982, *MNRAS*, 198, 1007
- Oemler, A., 1974, *ApJ*, 194, 1
- Oemler, A., 1992, in "Clusters and Superclusters of galaxies", Fabian A. C. ed. NATO Advanced Science Institutes (ASI) Series C, Volume 366, p.29
- Oemler, A., Dressler A., Butcher, H. R., 1997, *ApJ*, 474, 561
- Oke, J. B. et al. 1995, *PASP*, 107, 375
- Oke, J. B., Postman, M., Lubin, L. M., 1998, *AJ*, 116, 560
- Pimblet, K., Smail, I., Kodama, T., Couch, W.J., Edge, A.C., Zabludoff, A.I., O'Hely, E. 2002, *MNRAS*, 331, 333
- Poggianti, B. M., Smail, I., Dressler, A., Couch, W. J., Barger, A. J., Butcher, H., Ellis, R. S., Oemler, A., 1999, *ApJ*, 518, 576
- Postman, M., Lauer, T.R., Szapudi, I., Oegerle, W., 1998, *ApJ*, 506, 33
- Postman, M., Geller, M. J., *ApJ*, 281, 95
- Shigel, D. J., Finkbeiner, D. P., Davis, M., 1998, *ApJ*, 500, 525
- Simard, L. et al. 1999, *ApJ*, 519, 653
- Smail I., Ellis R. S., Dressler A., Couch W. J., Oemler A., Sharples R. M. & Butcher H. *ApJS*, 1997, 479, 70
- Soucail, G., Ota, N., Böringer, H., Czoske, O., Hattori, M., Mellier, Y. 2000, *A&A*, 355, 433
- Springel, V., White, S. D. M., Tormen, G., Kauffmann, G. 2001, *MNRAS*, 328, 726
- Stanford, S. A., Eisenhardt, P. R. M. & Dickinson, M. E. 1995, *ApJ*, 450, 512
- Stanford, S. A., Eisenhardt, P. R. M. & Dickinson, M. E. 1998, *ApJ*, 492, 461
- Toniazzo, T. & Schindler, S. 2001, *MNRAS*, 325, 509
- Treu, T., Stiavelli, M., Bertin G., Casertano, C., & Møller, P. 2001b, *MNRAS*, 326, 237
- Treu, T., Stiavelli, M., Casertano, C., Møller, P., & Bertin, G. 1999, *MNRAS*, 308, 1037
- Treu, T., Stiavelli, M., Casertano, C., Møller, P., & Bertin, G. 2002, *ApJ*, 564, L13
- Treu, T., Stiavelli, M., Møller, P., Casertano, C., & Bertin, G. 2001a, *MNRAS*, 326, 221
- van der Marel, R.P., Magorrian, J., Carlberg, R.G., Yee, H.K.C., Ellingson, E. 2000, *AJ*, 119, 2038
- van Dokkum P., Franx M., 1996, *MNRAS*, 281, 985
- van Dokkum, P. G., Franx, M., Kelson D. D. & Illingworth G. D., 1998a, *ApJ*, 504, L17
- van Dokkum, P. G., Franx, M., Kelson D. D. & Illingworth G. D., Fisher, D., Fabricant, D., 1998b, *ApJ*, 504, 714
- van Dokkum, P. G., Franx, M., Fabricant, D., Illingworth, G. D., & Kelson D. D. 2000, *ApJ*, 541, 95
- van Dokkum, P. G., Franx, M., Kelson D. D. & Illingworth, G. D., 2001, *ApJ*, 553, L39
- van Dokkum, P. G., Stanford, S. A., Holden, B. P., Eisenhardt P. R., Dickinson, M., Elston, R. 2001, *ApJ*, 552, L101
- Vitvitska M., Klypin, A. A., Kravtsov, A. V., Bullock J. S., Wechsler, R. H., Primack, J. R. 2002, *ApJ*, submitted (*astro-ph/0105349*)
- Valotto, C. A., Moore, B., Lambas, D. G. 2001, *ApJ*, 546, 157
- Vollmer, B., Cayatte, V., Balkowski, C., Duschl, W. J. 2001, *ApJ*, 561, 768
- Yee, H. K., Ellingson, E., Carlberg, R. G., 1996, *ApJS*, 102, 269
- Whitmore, B. C., & Gilmore, D. M. 1991, *ApJ*, 367, 64
- Whitmore, B. C., Gilmore, D. M., & Jones, C. 1993, *ApJ*, 407, 489
- Yee, H. K. C., Ellingson, E. & Carlberg, R. G. 1996, *ApJS*, 102, 269
- Zabludoff, A. I. & Franx, M., 1993, *AJ*, 106, 1314
- Ziegler B.L., Saglia, R.P., Bender, R., Belloni, P., Greggio, L., Seitz, S. 1999, *A&A*, 346, 13

TABLE C1
SUMMARY OF RELEVANT OBSERVED QUANTITIES FOR CLUSTER CL0024+16.

Observable	Value	Ref
r_c^a (X-ray)	10''4	(1)
β^b (X-ray)	0.475	(1)
L_X (X-ray)	$3.7 \cdot 10^{44}$ erg s ⁻¹	(2)
T_X (X-ray)	$5.7_{-2.1}^{+4.9}$ keV	(2)
center (X-ray)	00:26:36.3 17:09:46	(2)
center (galaxies)	00:26:34.8 17:10:05	(4)
center (BCG)	00:26:35.7 17:09:43	(0)
σ_∞	911 km s ⁻¹	(4)
R_{vir}	1.7 Mpc	(0)
Concentration	0.53	(3)

^aCore radius of the best-fitting β -model.

Note. — All coordinates are J2000. Data from (0) this paper ; (1) Böhringer et al. (2000); (2) Soucaill et al. (2000); (3) Dressler et al. 1997; (4) Girardi & Mezzetti 2001

TABLE C2
SUMMARY OF POINTINGS

POS	RA(J2000)	DEC(J2000)	PA_V3	exptime ^a	Ngal ^b	Nmorph ^c	Nz
00	00:26:37.4	+17:08:54.7	148.29	19800	508	188	77
01	00:27:01.5	+17:18:49.8	280.00	4400	269	41	2
02	00:26:47.0	+17:19:42.3	280.00	4400	266	51	5
03	00:26:32.6	+17:20:34.6	280.00	4400	262	44	4
04	00:27:12.3	+17:14:30.2	280.00	4400	267	31	3
05	00:26:56.8	+17:15:24.3	61.84	4000	279	55	8
06	00:26:46.4	+17:16:12.3	239.09	4400	280	58	17
07	00:26:27.8	+17:17:09.0	62.04	4000	252	61	16
08	00:26:13.4	+17:18:01.3	62.67	4000	249	53	6
09	00:27:23.2	+17:10:15.5	244.20	4400	256	46	0
10	00:27:08.4	+17:10:59.2	314.99	4400	286	45	3
11	00:26:53.1	+17:11:57.1	62.73	4000	270	54	11
12	00:26:39.8	+17:12:52.4	246.80	4400	275	51	17
13	00:26:24.2	+17:13:41.5	61.36	4000	292	82	17
14	00:26:10.8	+17:14:32.0	280.00	4400	296	49	6
15	00:25:56.4	+17:15:29.5	243.13	4400	395	53	0
16	00:27:18.9	+17:06:46.7	241.11	4400	331	61	0
17	00:27:04.5	+17:07:39.1	240.87	4400	350	60	0
18	00:26:53.2	+17:08:46.9	240.31	4400	290	48	13
19	00:26:21.3	+17:10:08.2	323.79	4400	280	58	15
20	00:26:06.1	+17:11:08.0	73.00	4000	226	36	4
21	00:25:51.6	+17:11:58.8	63.42	4000	299	54	0
22	00:27:14.8	+17:03:14.1	35.68	4400	319	54	3
23	00:26:45.8	+17:05:02.5	63.18	4000	292	49	3
24	00:26:32.5	+17:05:52.9	280.00	4400	288	48	9
25	00:26:16.9	+17:06:46.9	62.32	4000	263	48	10
26	00:26:02.5	+17:07:39.1	62.32	4000	273	42	4
27	00:25:48.2	+17:08:29.0	39.49	4000	285	51	0
28	00:26:56.6	+17:00:42.5	61.29	4000	273	62	5
29	00:26:27.7	+17:02:27.2	61.45	4000	293	40	12
30	00:26:14.4	+17:03:17.7	280.00	4400	309	63	10
31	00:25:58.8	+17:04:11.8	62.96	4000	290	50	4
32	00:26:41.1	+16:58:37.1	241.36	4400	341	76	3
33	00:26:24.7	+16:59:01.8	240.07	4400	270	41	3
34	00:26:10.2	+16:59:54.0	241.06	4400	325	55	8
35	00:26:03.3	+17:18:53.0	62.79	4000	301	69	6
36	00:26:30.8	+17:11:28.9	295.39	4400	357	108	40
37	00:26:43.6	+17:07:44.8	248.60	4400	342	61	12
38	00:26:29.9	+17:08:44.6	62.95	4000	384	111	40

^aTotal exposure time in seconds

^bTo $I = 25$

^cTo $I = 22.5$

Note. — For each pointing we list position, orientation, exposure time, number of objects detected, number of objects with morphological classification, and number of spectroscopic redshifts

TABLE C3
SUMMARY OF ENTRIES IN THE CATALOG

Entry	Description
POS	WFPC2 pointing, as identified in Table 2
chip	WFPC2 chip
ID	running number within each chip
X	x-coordinate on the chip of the object baricenter
Y	y-coordinate on the chip of the object baricenter
RA	Right Ascension (J2000) of the object baricenter
DEC	Declination (J2000) of the object baricenter
IAU	F814W mag_auto (SExtractor)
δ IAU	error on IAU (SExtractor)
IAP1	F814W magnitude within $0''.5$ diameter aperture (SExtractor)
δ IAP1	error on IAP1 (SExtractor)
IAP2	F814W magnitude within $1''$ diameter aperture (SExtractor)
δ IAP2	error on IAP2 (SExtractor)
star	class_star (SExtractor)
T	morphological type (RSE)
Comment	Comment by RSE

TABLE C4
FIRST ENTRIES OF THE CATALOG

POS	chip	ID	X	Y	RA	DEC	IAU \pm δ IAU	IAP1 \pm δ IAP1	IAP2 \pm δ IAP2	star	T	Comment
0	2	1	1370.99	57.35	6.65112	17.131149	21.344 \pm 0.006	24.385 \pm 0.016	23.528 \pm 0.013	0.0	9	-
0	2	2	1476.62	8.03	6.65148	17.129572	21.641 \pm 0.005	23.141 \pm 0.007	22.007 \pm 0.004	0.0	9	-
0	2	3	1079.62	28.92	6.65243	17.135000	23.953 \pm 0.030	24.890 \pm 0.023	24.240 \pm 0.023	0.0	-	-
0	2	4	114.58	21.22	6.65556	17.148020	23.801 \pm 0.025	25.039 \pm 0.026	24.112 \pm 0.021	0.0	-	-
0	2	5	46.78	19.46	6.65580	17.148932	23.012 \pm 0.012	23.924 \pm 0.012	23.282 \pm 0.011	0.0	-	-
0	2	6	1441.84	16.16	6.65148	17.130072	24.393 \pm 0.045	26.099 \pm 0.062	25.119 \pm 0.049	0.0	-	-
0	2	7	205.43	3.96	6.65552	17.146742	24.424 \pm 0.032	25.028 \pm 0.025	24.597 \pm 0.027	0.0	-	-
0	2	8	1321.63	9.76	6.65195	17.131672	22.189 \pm 0.011	24.743 \pm 0.021	23.298 \pm 0.011	0.0	4	edge

Note. — Standard SExtractor (Bertin & Arnouts 1996) parameters are indicated by their standard name, and a full description can be found in SExtractor user's handbook.